Avalanche dynamics in evolution, growth, and depinning models

Maya Paczuski,* Sergei Maslov,† and Per Bak‡
Department of Physics, Brookhaven National Laboratory, Upton, New York 11973
(Received 30 March 1995; revised manuscript received 4 August 1995)

The dynamics of complex systems in nature often occurs in terms of punctuations, or avalanches, rather than following a smooth, gradual path. A comprehensive theory of avalanche dynamics in models of growth, interface depinning, and evolution is presented. Specifically, we include the Bak-Sneppen evolution model, the Sneppen interface depinning model, the Zaitsev flux creep model, invasion percolation, and several other depinning models into a unified treatment encompassing a large class of far from equilibrium processes. The formation of fractal structures, the appearance of $1/f$ noise, diffusion with anomalous Hurst exponents, Lévy flights, and punctuated equilibria can all be related to the same underlying avalanche dynamics. This dynamics can be represented as a fractal in d spatial plus one temporal dimension. The complex state can be reached either by tuning a parameter, or it can be self-organized. We present two *exact* equations for the avalanche behavior in the latter case. (1) The slow approach to the critical attractor, i.e., the process of self-organization, is governed by a "gap" equation for the divergence of avalanche sizes. (2) The hierarchical structure of avalanches is described by an equation for the average number of sites covered by an avalanche. The exponent γ governing the approach to the critical state appears as a constant rather than as a critical exponent. In addition, the conservation of activity in the stationary state manifests itself through the superuniversal result $\eta = 0$. The exponent π for the Lévy flight jumps between subsequent active sites can be related to other critical exponents through a study of "backward avalanches." We develop a scaling theory that relates many of the critical exponents in this broad category of extremal models, representing different universality classes, to two basic exponents characterizing the fractal attractor. The exact equations and the derived set of scaling relations are consistent with numerical simulations of the above mentioned models.

PACS number(s): 05.40.+j, 64.60.Ak

I. INTRODUCTION

The term spatiotemporal complexity describes systems that contain information over a wide range of length and time scales [1]. Specifically, if such a system is studied through a magnifying glass, then, no matter what the level of magnification is, a variation of the image is seen as different parts of the system are viewed. Similarly, if the image of a local part of the system is averaged over a time window, different images are seen at different times, no matter how large the time window is. This contrasts with the behavior of ordered systems, or random systems, including chaotic ones, which become uniform when viewed at sufficiently large length or time scales.

The appearance of complexity in nature presents a fascinating, long-standing puzzle. In this article, a qualitative and quantitative theory for the dynamics of complex systems is presented in the context of simple mathematical models for biological evolution and growth phenomena far from equilibrium. Spatiotemporal complexity emerges as the result of avalanche dynamics in driven systems. We unify the origin of fractals, $1/f$ noise, Hurst exponents for anomalous diffusion, Lévy flights, and punctuated equilibrium behavior, and elucidate their relationships through analytical and numerical studies of simple models, defined in Sec. II. These phenomena are signatures of spatiotemporal complexity and are related via scaling relations to the fractal properties of the avalanches, as summarized in Table I.

We wish to focus on three general, empirical phenomena that are manifestations of complexity. First, Mandelbrot [2] has pointed out the widespread occurrence of self-similar, fractal behavior in nature. Mountains, coastlines, and perhaps even the Universe [3] have features at all scales. River networks consist of streams of all sizes [4]; the pattern of earthquake faults, cracks in rocks, or oil reservoirs is self-similar [5]. Second, noise with a $1/f^{\tilde{d}}$ power spectrum is emitted from a variety of sources, including light from quasars [6], river flow [7], and brain activity [8]. Third, many natural and social phenomena, including earthquakes, economic activity, and biological evolution appear to evolve intermittently, with bursts, or avalanches extending over a wide range of magnitudes, rather than smoothly and gradually. For instance, the distribution of earthquake magni-

*Electronic address: maya@cmt1.phy.bnl.gov
†Also at the Department of Physics, State University of New York at Stony Brook, Stony Brook, New York 11794. Electronic address: maslov@cmth.phy.bnl.gov
‡Electronic address: bak@cmth.phy.bnl.gov

TABLE I. Exponent relations for the extremal models in d dimensions. For invasion percolation, d should be replaced with the fractal dimension of the active boundary d_B except in the scaling relation for ρ (see text). The exponents τ_{ALL}, τ_{FIRST}, and $\tilde{d}$ are not defined for invasion percolation. In the interface models D is related to the interface roughness χ via $D = d + \chi$.

Exponent	Physical property	(ν and D)	(τ and D)
D	avalanche dimension	basic exponent	basic exponent
ν	correlation length	basic exponent	$\frac{1}{d-D(\tau-1)}$
τ	avalanche size distribution	$1+\frac{d-1/\nu}{D}$	basic exponent
γ	average avalanche size	$1+\nu(D-d)$	$\frac{2-\tau}{1+d/D-\tau}$
σ	avalanche cutoff	$1/\nu D$	$1+\frac{d}{D}-\tau$
ρ	relaxation to attractor	$\frac{1}{\nu(D-d)}$	$\frac{1+\frac{d}{D}-\tau}{1-d/D}$
η	average growth of activity	0	0
d_f	dimension of active sites	$d-\frac{1}{\nu}$	$D(\tau-1)$
z	dynamical exponent	$D-d+\frac{1}{\nu}$	$D(2-\tau)$
π	jump of minimal site	$1+D-d+\frac{1}{\nu}$	$1+D(2-\tau)$
τ_f^{all}	all forward avalanches	2	2
τ_b^{all}	all backward avalanches	$2-\frac{d-1/\nu}{D}$	$3-\tau$
τ_{FIRST}	punctuated equilibrium	$2-\frac{d}{D}$	$2-\frac{d}{D}$
τ_{ALL}	all returns	$\frac{d}{D}$	$\frac{d}{D}$
$\tilde{d}$	$1/f$ noise	$1-\frac{d}{D}$	$1-\frac{d}{D}$

tudes obeys the Gutenberg-Richter law [9]. Recent experiments on slowly driven sandpiles [10] and rice piles [11] show avalanches, or disturbances in the heap, of all sizes. Field *et al.* monitored the dynamics of superconducting vortices and found the superconducting analog of sandpile avalanches to be a power law over two decades [12]. Gould and Eldredge have proposed that biological evolution takes place in terms of punctuations, where many species become extinct and new species emerge, interrupting quiet periods of apparent equilibrium, known as stasis [13]. Large events, such as massive extinctions or even the large scale structure of the Universe, may have a statistical explanation as the power-law tail of a Lévy distribution. This is the case even though the large events are identifiable and tend to be viewed, erroneously we believe, as "atypical."

Even though spatiotemporal complexity is ubiquitous in nature, until recently little understanding of its origin has been achieved. One clear exception, though, are critical points for second order phase transitions in equilibrium systems, which are characterized by scale invariance. Borrowing the terminology from equilibrium thermodynamics, we shall also refer to systems with a large range of length and time scales as "critical." Spatial complexity occurs at the percolation transition in random bond or site models [14]; temporal complexity exists at the transition to chaos in the Feigenbaum map [15]. These systems are critical, and thus complex, as the result of tuning: the temperature, or some other parameter, is set to a specific value in order to achieve criticality. In nature, though, fine tuning of specific parameters is rare and unlikely; in addition, many systems in nature are far from an equilibrium state.

Thus another mechanism has been proposed; namely, systems that are far from equilibrium become critical through self-organization [16]. They evolve through transient states, which are not critical, to a dynamical attractor poised at criticality. In order for self-organization to occur, these systems must be driven slowly through a succession of metastable states. The system jumps from one metastable state to another by avalanche dynamics. These avalanches build up long-range correlations in the system. Here, we shall be mainly concerned with the self-organized critical (SOC) origin of spatiotemporal complexity. In some cases, though, similar considerations, such as scaling relations, can also be applied in cases where the criticality is tuned rather than self-organized. In particular, this is relevant for systems which undergo depinning transitions when a parameter is varied, such as interfaces, charge density wave systems, and superconducting flux lattices. In this case, too, long-lived metastable states are important and the dynamics is that of avalanches [17]. Avalanche dynamics in these tuned depinning transitions are discussed in Sec. VI.

SOC complements the concept of chaos, where simple systems with few degrees of freedom can display complicated behavior. Chaos is associated with a fractal "strange" attractor in phase space. These self-similar structures have little to do with fractals in large spatially extended systems that have many degrees of freedom. In addition, chaotic systems exhibit white noise (e.g., a positive Lyapunov exponent) with limited temporal correlations whereas complex systems have long-range spatiotemporal correlations.

From the earliest Bak-Tang-Wiesenfeld (BTW) sandpile models [16] and, later, earthquake models [18], most of the evidence for SOC behavior has been numerical. Exceptions include the work on singular diffusion by Carlson, Chayes, Grannan, and Swindle [19], and the one-dimensional forest fire model [20], where exact results have been found by Drossel, Clar, and Schwabl [21] and also by Paczuski and Bak [22]. Dhar [23] was able to char-

acterize the critical attractor of the BTW sandpile model in terms of an Abelian group, and thereby calculate the number of states on the attractor. With Ramaswamy, he solved a directed sandpile model exactly [24]. So far, though, none of the solutions of these different models have yielded a general phenomenology for SOC behavior. Most importantly, the fundamental mechanism for the self-organization process, via avalanches, has not been well understood. Pietronero and collaborators have developed a scheme, the fixed scale transformation [25], and applied it to a variety of nonequilibrium dynamical systems including diffusion limited aggregation [26], the sandpile models [27], and the Bak-Sneppen evolution model [28]. Here, we take a different approach where, based on certain exact results together with a scaling ansatz, we develop a theory that relates different critical exponents, including the approach to the attractor, to two basic exponents which are model dependent.

A common feature of many models exhibiting SOC is the selection of extremal sites for the initiation of events, rather than statistically typical sites. This feature of extremal dynamics has been somewhat obscured by the introduction of models, such as the BTW sandpile model or the forest fire model, which appear to be driven randomly. In the "random" BTW model, sand is added to random sites until a local threshold is exceeded and a toppling occurs. However, the statistics of avalanches in the BTW model is not changed in "deterministic" versions where the height of every site is raised uniformly until one site, the least stable site, topples. In the latter case, randomness only enters into the initial conditions. One might say that in the "random" BTW model the system selects the extremal sites itself, while in the "deterministic" case it is forced to do so. Similarly, in the Olami, Feder, and Christensen earthquake model [18], the force is raised uniformly until the site with the largest force ruptures. Zaitsev [29] introduced a model for low temperature flux creep where the motion always takes place at the site with the largest force, and showed that the model self-organizes to a critical state. In the forest fire model, it can be shown rigorously that the process is driven by the burning of the largest forests with the oldest trees, despite the fact that the trees grow randomly [21,22]. Again, burning trees randomly only serves as a vehicle for the system to burn the largest forests. In a remarkable paper, Miller *et al.* [30] suggested through a different line of thinking that $1/f$ noise and fractality are related to the preferential selection and thermal activation of extremal sites.

Recently, a variety of simple models with extremal dynamics that exhibit SOC have been introduced. These models, including the Bak-Sneppen evolution model [31], the Sneppen interface depinning model [32], and the Zaitsev model [29], are defined in Sec. II. They are driven by sequentially updating the site with globally extremal values of the signal. This information is propagated through the system via local interactions. These models, representing different universality classes, are nevertheless similar to invasion percolation [33,34]. Interestingly, invasion percolation was recognized as a SOC phenomenon by Roux and Guyon [35] some years ago. These authors, inspired by the sandpile analogy [16], defined avalanches in invasion percolation in terms of a fluctuating extremal signal. Some additional new results for invasion percolation have recently been presented by Maslov [36] using methods similar to those applied in this work.

Our main analytical results for this class of models, including invasion percolation, are encapsulated by two exact equations plus a superuniversal scaling law for stationary critical processes. These results address basic questions that arise in SOC. Perhaps the most obvious question is how the system self-organizes into the complex, critical state. This is described by a "gap" equation that relates the rate of approach to the attractor to the average avalanche size [37]. This equation demonstrates that the stationary state of the system is a critical state for the avalanches, where the average avalanche size diverges. Assuming that this divergence has a characteristic exponent γ, we show from the gap equation that the system approaches its attractor algebraically with a characteristic exponent, $\rho = 1/(\gamma - 1)$, for the transient.

The off-critical exponent for the transient, γ, can be expressed in terms of the exponents in the stationary state itself, via a "γ" equation for the hierarchy of avalanches [38]. This may result from the fact that the off-critical direction is stable (in SOC the critical point is an attractor for the dynamics) rather than being unstable. Lastly, in SOC the critical point is constrained to be stationary. This leads to a fundamental law for the critical states; $\eta = 0$ in all dimensions [39]. One dramatic consequence of this law is that the fractal dimension of the active sites, d_f, is fixed by the probability distribution for avalanche sizes in the stationary state, i.e., $d_f = D(\tau - 1)$. Thus the widespread appearance of fractal structures can, perhaps, be viewed as a consequence of the existence of a stationary limit.

By studying the space-time behavior of the activity pattern in the critical state, i.e., the spatial location of the extremal site at a particular point in time, one can describe the activity pattern as a fractal embedded in d spatial dimensions plus one temporal dimension [40]. This fractal has a mass dimension or avalanche dimension D. Long-range time correlations, e.g., $1/f$ noise, and spatial fractal behavior are unified as different cuts in this underlying space-time fractal. The temporal evolution at a specific position is expressed as the activity along a one dimensional time line piercing the fractal perpendicular to the spatial dimensions. The fractal spatial structure is found by cutting the fractal along the spatial directions at that time. We establish a formal relation between $1/f$ type noise and fractal spatial behavior in terms of the avalanche dimension D. In the critical state, the dynamics is best characterized in terms of scale-free avalanches, initiated at extremal sites, and propagating by an anomalous diffusion process. Figure 1 shows this space-time fractal for the one-dimensional evolution model.

We have studied, in more detail, the value of the extremal signal in time. Time directed avalanches are naturally defined in terms of this fluctuating signal [36]. These avalanches have a hierarchical structure of valleys within valleys. Forward and backward time directed avalanches have different statistical distributions in the

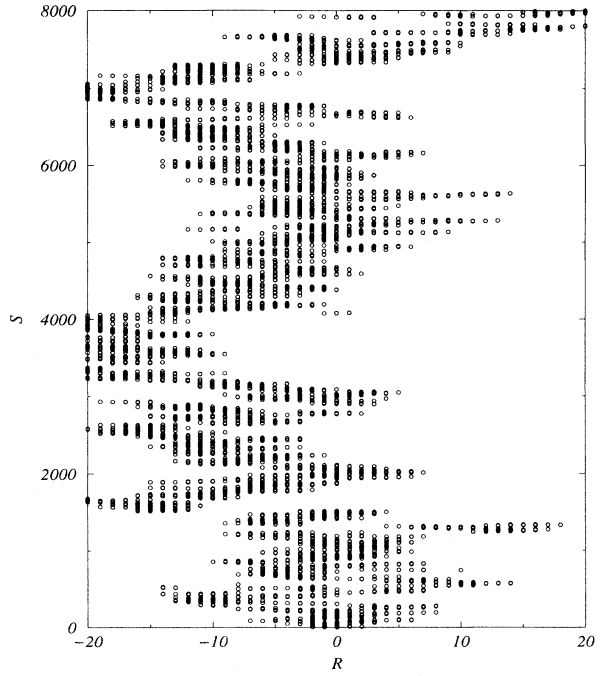

FIG. 1. The space-time fractal activity pattern for the one-dimensional evolution model. Time is measured as the number of update steps, S.

stationary state, reflecting the irreversibility of extremal processes. The distribution of all forward avalanches, starting at each update step for the extremal dynamics, is a power law with a superuniversal exponent $\tau_f^{all} = 2$. The distribution of all backward avalanches is also a power law, but with a different model dependent exponent $\tau_b^{all} = 3 - \tau$, where τ is the usual avalanche size distribution exponent.

Taken together, these considerations lead to many scaling relations for various physical quantities. All of the critical exponents that we consider can be expressed in terms of two basic exponents, for instance, the avalanche dimension D, and τ, which characterizes the distribution of avalanche sizes. These scaling relations are summarized in Table I. They provide numerous points to test theoretical predictions with numerical simulations of different models. We have made numerical tests of essentially all the scaling relations for many of the models and find a pattern of consistency which confirms the predicted scaling relations across different universality classes; nevertheless, more accurate tests are needed for any specific result. The results of our simulations are presented in Table II, and the error bars represent statistical errors for system sizes studied. We urge that extensive, accurate simulations be performed. Indeed, others [41,42] have already provided further confirmation of our scaling relations.

It is important to note that for some models the critical point can be reached in different ways. This is especially clear in the context of depinning. The depinning transition can be self-organized or reached by tuning either an external driving force or the velocity. In the context of interface depinning and invasion percolation, the SOC version corresponds to driving at constant velocity in the limit where the velocity vanishes. Some of the exponents are the same in the different cases but others, in general, are different. For example, $\eta = 0$ for all SOC depinning models, but may be nonzero for the depinning transition at constant driving force. The critical points that are reached by the self-organizing process are different from the critical points that are reached in an equivalent model by tuning a driving force. Thus, despite the fact that these differences disappear in mean field theory, SOC cannot, even in principle, be viewed as sweeping a system through a critical point, in contrast to the claims in Ref. [43]. The similarities and differences between constant force and SOC depinning are elaborated in Sec. VI.

TABLE II. Critical exponents measured and illustrated in figures throughout the text. All values were determined independently. ( ) indicates uncertainty in the last digit. Within these uncertainties, all exponents are consistent with the exponent relations from Table I.

Exponent	Bak-Sneppen model		Linear interface model		Sneppen model
	1 dimension	2 dimensions	1 dimension	2 dimensions	1 dimension
	$f_c = 0.66702(3)$	$f_c = 0.328855(4)$			$f_c = 0.4614(4)$
D	2.43(1)	2.92(2)	2.23(3)	2.725(20)	
τ	1.07(1)	1.245(10)	1.13(2)	1.29(2)	1.26(1)
γ	2.70(1)	1.70(1)			2.13(20)
π	3.23(2)		2.93(3)	2.89(3)	
η	0.01(2)	0.000(2)	0.000(6)[a]		0.03(5)
d_s	0.11(2)	0.250(5)	0.15(3)[a]		0.26(2)
z	2.10(5)	2.17(2)			1.19(5)[b]
τ_{FIRST}	1.58(2)	1.28(3)			
τ_{ALL}	0.42(2)	0.70(3)			
$\tilde{d}$	0.58(3)[c]	0.31(3)[c]			

[a]Measured for 1D Zaitsev model, presumably from the same universality class [56].

[b]This exponent for the TLB model (parallel analog of Sneppen model) was measured to be 1.00 ± 0.05.

[c]This exponent was measured from the power spectrum of activity.

Our scaling relations are compared with recent numerical simulations for constant force depinning [44,45].

Self-organized fractal growth is fundamentally different from growth processes that are, for example, described by (variants of) the Kardar-Parisi-Zhang (KPZ) equation [46,47]. The KPZ equation is scale invariant by symmetry, and thus the criticality is not self-organized. It is essential to have long-lived, metastable states for the self-organization process to take place through avalanches, without reverting to a "ground state" at or near equilibrium. In addition, unlike "generic scale invariance" [47], SOC does not require local conservation laws. With the exception of the Zaitsev model, all of the models we consider here are nonconservative; in spite of this, they can be shown to self-organize to a critical state. In the context of interface growth, the dynamic scaling approach has been used to separate avalanche dynamics associated with SOC and Langevin dynamics associated with generic scale invariance into distinct phenomenological categories [48].

Here, we present a comprehensive and detailed account of our work on the Sneppen interface model, the Bak-Sneppen evolution model, invasion percolation, and other SOC (and non-SOC) critical models, including interface depinning. Some of these results have been previously published in short accounts. For clarity, we provide here a complete, self-contained discussion of these models and our most accurate and extensive numerical results.

Section II introduces the models for the general reader. Section III examines the transient self-organization process and introduces the "gap" equation. Section IV discusses the avalanche hierarchy in the stationary state. In particular we present the "γ" equation, the law for stationary states, $\eta = 0$, and a discussion of time directed avalanches. The concept of backward avalanches is used to determine the exponent π governing the distribution of jumps in the activity, which has a Lévy distribution. Section V unifies spatial fractal behavior with $1/f$ type noise. Section VI contains our results on interface depinning. In the concluding section, the scaling relations that we derive and our numerical results are summarized. The Appendix explains in more detail the results for invasion percolation.

II. DEFINITION OF THE MODELS

In this section, we define all of the models studied here.

Evolution [31]. The Bak-Sneppen evolution model is perhaps the simplest model of SOC. In this "toy" evolution model, random numbers f_i are assigned independently to each site on a d-dimensional lattice of linear size L. They are chosen from a uniform distribution between zero and 1, $\mathcal{P}(f)$. At each update step, the extremal site, i.e., the one with the smallest random number f_{min}, is located. That site, and its $2d$ nearest neighbors are then assigned new random numbers, drawn independently from the flat distribution $\mathcal{P}$. After many updates have occurred, the system reaches a statistically stationary state in which the density of random numbers in the system vanishes for $f < f_c$ and is uniform above f_c. In the thermodynamic $L \to \infty$ limit, no random number with $f > f_c$ is ever the extremal site. A snapshot of the stationary state in a finite one-dimensional system is shown in Fig. 2. Except for a localized region, the avalanche, where there are small random numbers, all the random numbers in the system have values above the self-organized threshold $f_c = 0.667\,02 \pm 0.000\,03$ in one dimension.

The evolution model exhibits punctuated equilibrium behavior as does real biology [13]. It simulates evolutionary activity in terms of mutations of individual species and their interdependencies in a food chain. The random numbers represent the fitness of a species, and choosing the smallest random number mimics the "Darwinian" principle that the least fit species is replaced or mutates. The dynamical impact of the mutation of the least fit species on the rest of the ecology is simulated by changing the fitness of neighboring species on the lattice. Discussions of its possible connection to biological evolution and macroeconomics may be found in Refs. [31,49], and a mean field analysis in [50–52]. A generalized M-trait model where each species has many (M) internal degrees of freedom has very recently been introduced and solved exactly [53] in the $M \to \infty$ limit.

Sneppen [32]. In the Sneppen interface model for SOC depinning, an interface of size L^d defined on a discrete lattice $(\vec{x}, h)$ moves under the influence of quenched random pinning forces $f(\vec{x}, h)$ assigned independently from the flat distribution $\mathcal{P}$. Initially, $h(\vec{x}) = 0$. Growth occurs by advancing the extremal site on the interface with the smallest random pinning force f_{min} by one step. Then a constraint is imposed for all nearest neighbor gradients, $|h(\vec{x}) - h(\vec{x}')| \leq 1$. This is met by advancing the heights of neighboring sites. The process is repeated indefinitely. Like the evolution model, the Sneppen model also reaches a statistically stationary state where the den-

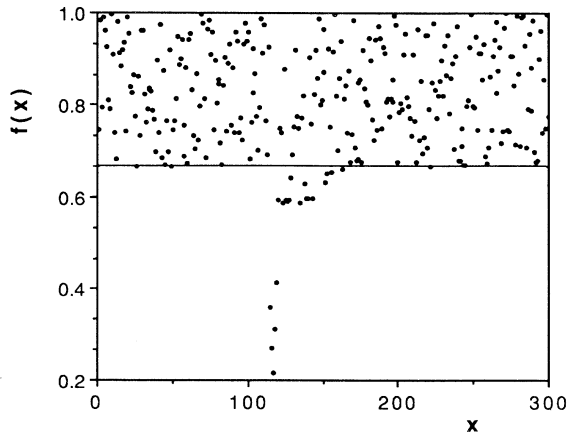

FIG. 2. Snapshot of the stationary state for the evolution model in a finite one-dimensional system. Except for a localized region, the avalanche, where there are small random numbers, all the random numbers in the system have values above the self-organized threshold $f_c = 0.667\,02$.

sity of random pinning forces on the interface vanishes for $f < f_c$ and is uniform above f_c. In this state, the interface moves in bursts of localized activity, as indicated schematically in Fig. 3. Outside these regions of activity, the interface is frozen for potentially long periods of time until a burst moves into the frozen region. The interface moves in a jerky, irregular manner, rather than smoothly and gradually advancing as a whole.

Tang and Leschhorn [54] showed that the one-dimensional model, in the stationary state, identifies from time to time with paths on a critical directed percolation cluster. It has been proposed that this identification with blocking paths can be used to obtain all of the critical exponents in terms of two independent exponents [55]. The identification with "blocking surfaces" is analogous to invasion percolation, where the invading region identifies from time to time with a critical cluster of ordinary percolation [33,35]. Possible physical realizations of the Sneppen model and other interface depinning models are discussed in Sec. VI.

Zaitsev [29]. Zaitsev introduced an extremal model for flux creep. Random numbers f_i, chosen from $\mathcal{P}$, are assigned independently to each site on a d-dimensional lattice of linear size L. At each update step, the site with the largest number is chosen, and a random number chosen from $\mathcal{P}$ is subtracted from that site and equally distributed to the $2d$ nearest neighbors. The activity conserves the sum of all the random numbers in the system. It has been suggested [56] that this model is in the same universality class as a self-organized "linear" interface depinning model (LIM), sometimes referred to as the quenched Edwards-Wilkins [57] equation.

"Linear" interface model. In the linear interface depinning model, the force at each site has a random contribution $f(\vec{x}, h)$ chosen from $\mathcal{P}$ to represent quenched random pinning forces, plus a linear configurational term $f_{conf} \sim \nabla^2 h$, where h is the local height and ∇^2 represents a discretized Laplacian. Thus the local internal force is

$$F_{int}(\vec{x}, t) = \nabla^2 h(\vec{x}, t) + f(\vec{x}, h(\vec{x}, t)) \ . \qquad (1)$$

We consider cases where this model is driven either (a) with extremal dynamics [40,56] or (b) in a parallel non-self-organized mode [58]. In (a) the site with the maximum total force is advanced by one unit, leading to SOC, or constant velocity depinning. In (b) the model may be tuned to a depinning transition by adding an external driving force F to all sites and advancing in parallel every site where the total force $(F_{int} + F)$ is positive by one step. When $F > F_c$ the interface moves with a finite velocity, while for $F < F_c$ it becomes stuck in a metastable state. At $F = F_c$ it undergoes a depinning transition. A tuned depinning transition may also be realized by externally setting the velocity v of the interface and allowing the force F to fluctuate so as to maintain that velocity. The stationary state of the SOC version corresponds to the depinning transition at constant velocity. The SOC version tunes itself to a constant velocity depinning transition. In Sec. VI, a comparison is made between the LIM and models for fluid invasion in porous media [59,60] and interface depinning in the random field Ising model [61]. There, it is also argued that τ and D are the same for the (constant force) tuned and SOC variants, but η and other dynamical exponents (e.g., d_f and z) can be different.

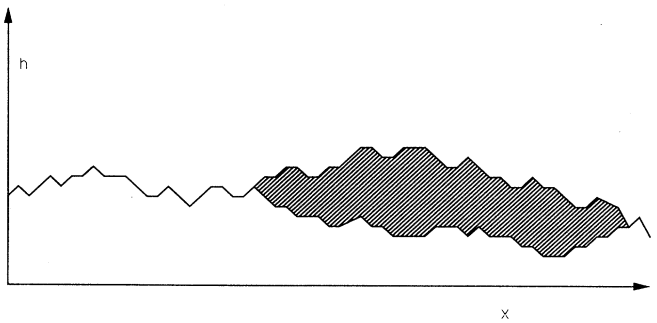

FIG. 3. Schematic picture of an avalanche separating two interface configurations in the Sneppen model. The size S of the avalanche corresponds to the shaded area.

Tang-Leschhorn-Buldyrev (TLB) model. A model for depinning of an elastic interface at constant force was studied by Tang-Leschhorn [62] and also by Buldyrev *et al.* [45]. Again, an interface of size L^d defined on a discrete lattice $(\vec{x}, h)$ moves under the influence of random pinning forces $f(\vec{x}, h)$ assigned independently from $\mathcal{P}$. Initially, $h(\vec{x}) = 0$. Instead of advancing the most unstable site, as in the Sneppen model, all unstable sites with $f < F$ are advanced in parallel. Then the constraint is imposed for all nearest neighbor gradients, $|h(\vec{x}) - h(\vec{x}')| \leq 1$. The system is relaxed to meet the gradient constraint. When $F = F_c$ the interface undergoes a depinning transition. Tang and Leschhorn [54,62] showed that in the critical state both the TLB model and the Sneppen model, in one dimension, identify with a directed percolation cluster of sites with $f > f_c$. In Sec. VI, it is argued that the exponents τ and D are the same for the TLB and Sneppen models; while η, z, and other dynamical exponents can be different.

Directed percolation (DP). In directed percolation, a preferred direction, labeled by t, is chosen and bonds are oriented with respect to t. Percolation is only allowed in the direction of increasing t. Each bond exists with probability f. When $f = f_c$, the DP cluster can become infinitely large. This model can be viewed as the "parallel" constant force version of the evolution model. In DP, there is a critical point which is tuned.

Invasion percolation [33,34]. Invasion percolation is the oldest member of this class of models. It was studied as a SOC phenomenon, in terms of avalanches, by Roux and Guyon [35]. In invasion percolation, random numbers f_i are assigned independently to each site on a $(d+1)$-dimensional lattice of linear size L. They are chosen from a uniform distribution between zero and 1, $\mathcal{P}(f)$. Initially, one d-dimensional side of the lattice is the "invaded cluster." The random numbers at the boundary of the invaded cluster are examined. At each update step, the extremal site, i.e., the site with the smallest random number f_{min} on the boundary of the invaded cluster is located. That site is then invaded, and new sites susceptible to growth are added to the boundary.

The universality class of the model is sensitive to the exact definition of the boundary. Models with different definitions of the boundary (IP-1, IP-2, IP-3) are given in the Appendix, along with a discussion of their physical realizations.

III. SELF-ORGANIZATION

Self-organization, as used here, refers to a dynamical process whereby a system starts in a state with uncorrelated behavior and ends up in a complex state with a high degree of correlation. The time that it takes to self-organize grows as the system size increases, so that for large systems self-organization is a slow process. In contrast to the earlier models of SOC, the process of self-organization in the extremal models that are discussed here is very well understood. The stationary state is critical and is approached algebraically, through a sequence of transient states. In order to demonstrate this, we shall first discuss self-organization in the context of the evolution model, which has been defined in Sec. II, and then generalize the results to other models.

Let us consider the situation where the distribution of f's initially is uniform in the interval $[0,1]$ in a d-dimensional evolution model of linear size L. Initially, the activity, i.e., the spatial location of the smallest random number in time, jumps randomly throughout the system. Eventually, after a long transient, the system reaches a complex state where the activity is correlated, as shown in Fig. 1. In order to study this transient process, we examine the value of the minimal random number chosen, f_{min}, as a function of sequential time s, or the total number of updates. This signal $f_{min}(s)$ can be related to the distribution of random numbers in the system.

The first value $f_{min}(0)$ to be chosen for updating is $O(L^{-d})$. Since, by definition, there are no random numbers in the system smaller than $f_{min}(0)$, this quantity is defined to be the initial value of the gap, G, in the distribution of f's; that is, $G(0) = f_{min}(0)$. Eventually, after s updates, a larger gap $G(s) > G(0)$ opens up. The density of sites with random numbers below G vanishes in the thermodynamic $L \to \infty$ limit, and is uniform above G. The current gap $G(s)$ is the maximum of all the minimum random numbers chosen, $f_{min}(s')$, for all $0 \le s' \le s$. Figure 4 shows f_{min} as a function of s during the transient for a small system. The solid line shows the gap $G(s)$ as a stepwise increasing function of s. The gap is an envelope function that tracks the increasing peaks in f_{min}. Clearly, when the gap jumps to a new higher value, there are no sites in the system with random numbers less than the gap. Since the distribution $P(f)$ that each of the random numbers are chosen from is flat, all of the random numbers in the system are uniformly distributed in the interval $[G(s),1]$ at those moments in time when the gap jumps. Thus the envelope function tracks the distribution of random numbers in the system.

By definition, the separate instances when the gap $G(s)$ jumps to its next higher value are separated by avalanches. Avalanches correspond to plateaus in G during which $f_{min}(s) < G(s)$. This guarantees that the events within a single avalanche are causally and spatially connected. A new avalanche is initiated every time the gap jumps, and all the consecutive random numbers which are smaller than the gap after this event must have originated from the site that started the new avalanche. Once an avalanche is over it does not affect the behavior of any subsequent avalanche, except in terms of the gap threshold. As the gap increases, the probability for the new random numbers to fall below the gap increases also, and longer and longer avalanches typically occur.

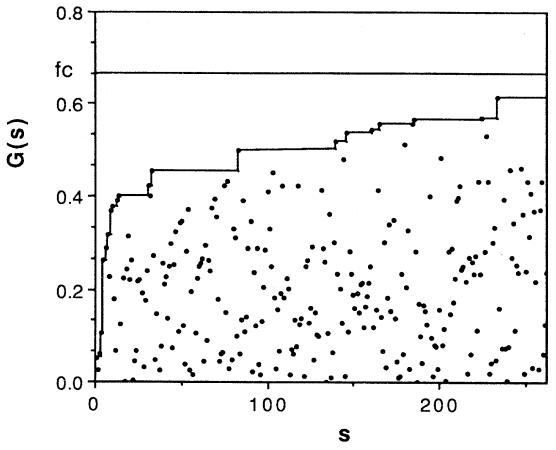

FIG. 4. Value of the extremal signal f_{min} as a function of s during the transient in a small ($L = 20$) one-dimensional evolution model. The full line shows the gap $G(s)$ as a stepwise increasing function of s. The gap is an envelope function that tracks the peaks in f_{min}.

Since the distribution of random numbers above the gap is flat, the average size of the jump in the gap at the completion of each avalanche is $[1 - G(s)]/L^d$. The other quantity that is needed in order to describe the self-organizing system is the average size of the plateau for a given value of G, or the average avalanche size $\langle S\rangle_{G(s)}$. We shall prove below that in the limit of large system sizes L the growth of the gap versus time s obeys the exact gap equation [37]

$$\frac{dG(s)}{ds} = \frac{1 - G(s)}{L^d \langle S\rangle_{G(s)}} . \tag{2}$$

As the gap increases, so does the average avalanche size $\langle S\rangle_{G(s)}$, which eventually diverges as $G(s) \to f_c$, whereupon the model is critical and the process achieves stationarity. In the limit $L \to \infty$, the density of sites with $f < f_c$ vanishes, and the distribution of f's is uniform above f_c. The gap equation (2) defines the mechanism of approach to the self-organized critical attractor. It contains the essential physics of SOC phenomena. When the average avalanche size diverges, $\langle S\rangle_{G(s)} \to \infty$, the system becomes critical. At the same time, $\frac{dG}{ds}$ approaches zero,

which means that the system becomes stationary. Examining Eq. (2) one notices another mathematical possibility for the stationary limit, which does not require diverging avalanches. The time derivative $\frac{dG}{ds}$ is exactly zero if the current gap $G(s) = 1$. This situation, however, is not realized in any extremal model in the limit that $L \to \infty$, since the presence of any interaction between sites (such as replacing nearest neighbors with new random numbers in the evolution model) will result in $f_c < 1$.

We prove the gap equation as follows. For any selected resolution $\Delta G \ll 1$ along the gap axis there is a system size L sufficiently large that many avalanches are needed to increase the gap from $G(s)$ to $G(s) + \Delta G$. In this case, the sum of (a) the temporal durations S of an individual avalanche and (b) the jumps in the gap at the end of each avalanche will both average within this interval because they are both sums of independent random variables. Therefore, in the limit $L \to \infty$ Eq. (2) is exact. To be more specific, suppose that the current value of the gap in the system is $G(s)$. The average number of avalanches required to increase the gap by ΔG is $N_{av} = \Delta G L^d/[1 - G(s)]$. By selecting system size $L \gg \Delta G^{-1/d}$ we ensure that $N_{av} \gg 1$. N_{av} can be made arbitrarily large by taking the large L limit. In this limit, the average number of time steps required to increase the gap from $G(s)$ to $G(s) + \Delta G$ is given by the interval $\Delta s = \langle S \rangle_{G(s)} N_{av} = \langle S \rangle_{G(s)} \Delta G L^d/[1 - G(s)]$, and from the law of large numbers the fluctuations of this interval around its average value vanish. This equation shows that the ratio of the interval length Δs to the time s required to reach $G(s)$, $\Delta s/s$, vanishes as $\Delta G \to 0$. Rewriting the interval equation as $\frac{\Delta G}{\Delta s} = \frac{1-G(s)}{L^d \langle S \rangle_{G(s)}}$ and taking the continuum limit we restore the differential equation (2).

In order to solve the gap equation we need to know precisely how the average avalanche size $\langle S \rangle_{G(s)}$ diverges as the critical state is approached. It is natural to assume that this divergence has a power-law form. In analogy with percolation clusters, we now make an ansatz that the average avalanche size diverges as G approaches f_c as

$$\langle S \rangle \sim (f_c - G)^{-\gamma} . \tag{3}$$

We will show in the next section that for the extremal models studied here the exponent $\gamma \geq 1$. Let us first consider the case $\gamma > 1$. Inserting Eq. (3) into Eq. (2) and integrating, one obtains

$$\Delta f = f_c - G(s) \sim \left(\frac{s}{L^d}\right)^{-\rho} \quad \text{where } \rho = \frac{1}{\gamma - 1} . \tag{4}$$

Equation (4), first derived in [37], was also found by Ray and Jan [51]. It shows that the critical point ($\Delta f = 0$) is approached algebraically with an exponent $-\frac{1}{\gamma-1}$. Equation (4) holds over the range $L^d \ll s \ll L^{\tilde{D}}$. The lower limit requires that the avalanches are in the scaling regime, so that Eq. (3) is valid. The upper limit requires that the cutoff $r_{co} \sim \Delta f^{-\nu}$ in the spatial extent of the avalanches is much less than the system size, or $\Delta f^{-\nu} \ll L$. Inserting Eq. (4) into this expression gives

$$\tilde{D} = d + \frac{\gamma - 1}{\nu} . \tag{5}$$

The boundary case $\gamma = 1$, realized, for instance, in the mean field version of the evolution model [50–52], results in an exponential relaxation to the critical attractor:

$$\Delta f \sim e^{-As/L^d} , \tag{6}$$

where A is a numerical constant that is independent of L. This expression is valid as long as $L^d \ll s \ll L^d \ln L$, and the system reaches the stationary state when $s \sim L^d \ln L$.

It is straightforward to demonstrate, in a step by step fashion, that the gap equation (2) holds not only for the self-organization process in the evolution model, but also for the Sneppen interface model [55]. For the self-organized LIM and the Zaitsev model, the distribution of internal forces in the system is not given by a flat distribution, unlike the evolution and Sneppen models. However, the extremal dynamics allows one to define a fluctuating signal $f_{min}(s)$ and therefore a gap function $G(s)$ as above. Now, though, the average size in the jumps of the gap is not given simply by $[1 - G(s)]/L^d$. However, as long as the distribution of internal forces above the gap is not singular, when the avalanche is finished, then a weaker form of the gap equation holds,

$$\frac{dG(s)}{ds} \sim \frac{1}{L^d \langle S \rangle_{G(s)}} . \tag{7}$$

If the scaling ansatz Eq. (3) holds, then depending on the value of γ either Eq. (4) or Eq. (6) describes the approach to the critical state.

For $(d+1)$-dimensional invasion percolation, the situation is slightly more complicated. During the transient process, the size of the boundary where growth may occur is growing. It can be shown [35] that, during the transient period of invasion percolation starting from a flat configuration, the active boundary $b(s)$ of the invading cluster scales with the invaded volume s as

$$b(s)/L^d \sim (s/L^d)^g = (s/L^d)^{\frac{d_B - d}{D - d}} . \tag{8}$$

Here, d_B is the fractal dimension of the boundary where growth may occur and D is the fractal dimension of the invaded cluster. The derivation of this equation is explained in the Appendix. The system reaches a stationary state when $s \sim L^D$. At this point, the size of the active boundary also reaches its finite size limit L^{d_B}. The proper gap equation for invasion percolation, taking into account the growth of the active boundary with time, can be written as

$$\frac{dG(s)}{ds} \sim \frac{1}{L^d (s/L^d)^g \langle S \rangle_{G(s)}} . \tag{9}$$

In the asymptotic critical region, the scaling ansatz Eq. (3) can be inserted into the gap equation (9). Integration gives

$$\Delta f = f_c - G(s) = \left(\frac{s}{L^d}\right)^{-\frac{1-g}{\gamma-1}}, \qquad (10)$$

which holds for $L^d \ll s \ll L^{d+\frac{\gamma-1}{\nu(1-g)}}$.

The scaling relations between these and other exponents are explained in the next section. One might naively suspect that the critical exponent γ would be an independent exponent describing off-critical behavior. This is not the case. The results of the next section allow us to determine γ in terms of the avalanche dimension D, and the avalanche distribution exponent τ, and solve the gap equation.

IV. PROPERTIES OF THE STATIONARY, CRITICAL STATE

In all previous SOC models, like, for instance, the BTW sandpile model [16] or the earthquake models [18], self-organized criticality manifested itself in a power-law distribution of bursts of activity, or avalanches, following a single perturbation. The new series of extremal SOC models is not an exception. In fact, avalanches in these models have an additional hierarchical structure of subavalanches within avalanches. In this section, avalanches in the stationary state are defined and related to the avalanches in the transient process defined in the previous section. This enables us to determine the exponent γ, characterizing the transient, in terms of the stationary probability distribution of avalanches. The hierarchical avalanche structure is revealed in the "γ" equation [38]. We then demonstrate the law for stationary states, $\eta = 0$ [39]. This law implies, among other things, that the fractal dimension of active sites is also determined by the stationary probability distribution for avalanches through the scaling relation $d_f = D(\tau - 1)$. All of the above mentioned results hold for forward avalanches; we close this section with a discussion of backward avalanches [36], and a derivation of a scaling relation for the Lévy flight exponent $\pi = 1 + D(2 - \tau)$.

Avalanches in the stationary state can be defined for any of the extremal models as follows. Suppose that at time s the smallest random number in the system was larger than f_0, where $0 < f_0 < 1$ is an auxiliary parameter used to define avalanches. Each of the new random numbers introduced at this time step can be smaller than f_0 with probability f_0 [for the flat distribution $\mathcal{P}(f)$]. According to the rules of the model, if one (or more) of the new random numbers is less than f_0, the smallest of those will be selected at the next time step $(s + 1)$. This initiates a creation-annihilation branching process, where the sites with $f_i < f_0$ play the role of particles, and the particle with the smallest random number is chosen for updating at each time step. While the avalanche continues to run, there is at least one such "particle" and the global, minimal random number is smaller than f_0. The avalanche stops, say at time $S + s$, when the last "particle" with a random number smaller than f_0 is eliminated. By definition, the global, minimal random number at this time step will be larger than f_0 once again. Thus one can view the parameter f_0 as a branching probability for the creation of particles. We will call the avalanches, defined by this rule, f_0 avalanches. They can be easily extracted from the *temporal signal* of the model $f_{min}(s)$, which is the value of the selected minimal number as a function of time s. In terms of this signal, the size of an f_0 avalanche is the number of time steps elapsed between subsequent punctuations of the barrier f_0 by the signal f_{min}. For the example given here, the size of the avalanche is S. The hierarchical structure of f_0 avalanches is demonstrated in Fig. 5.

The statistics of the avalanches clearly depends on the value of the branching probability f_0. The larger it is, the larger is the expected size of the avalanche. In analogy with ordinary percolation [63], there must be a critical value $f_c < 1$ of the branching probability such that the expected size of the f_c avalanche cluster becomes infinite. That means that in the thermodynamic limit $L \to \infty$ in the stationary state of the system, with probability 1, at least one "particle" with $f_i < f_c$ will exist, and the signal f_{min} will be smaller than f_c, also with probability 1. In analogy with ordinary percolation [63] and other "branching processes" such as directed percolation [14], a variety of nonequilibrium lattice models [64], or the propagation of an avalanche in the BTW sandpile model [16], we use the following scaling ansatz for the probability distribution $P(S, f_0)$ of f_0 avalanches of size S:

$$P(S, f_0) = S^{-\tau} g(S(f_c - f_0)^{1/\sigma}). \qquad (11)$$

Here, τ and σ are model dependent exponents and $g(x)$ is a scaling function, which decays rapidly to zero when $x \gg 1$ and goes to a constant when $x \to 0$. This scaling ansatz for various models has been confirmed by numerical simulations in [31,51,52,54,60,61]. When the auxiliary parameter f_0 is selected to be equal to f_c, the avalanche distribution is a power law $P(S) \sim S^{-\tau}$ without cutoff. When the parameter f_0 is lowered below f_c these critical

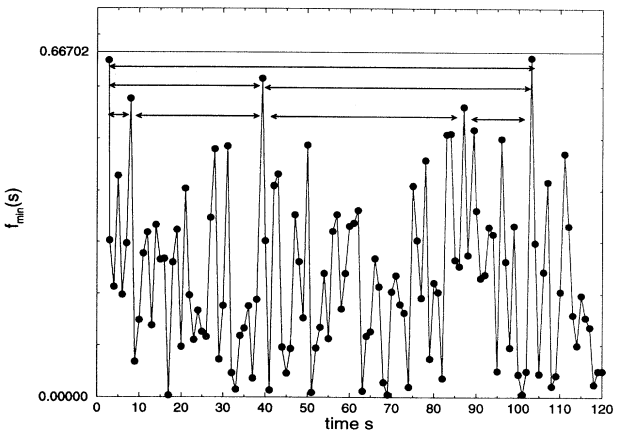

FIG. 5. Illustration of the hierarchical structure of the f_0 avalanches. The big avalanche is subdivided into smaller ones as the auxiliary parameter f_0 is lowered. The lines span f_0 avalanches for $f_0 = 0.63, 0.59$, and 0.54, respectively.

avalanches are subdivided into smaller ones and acquire a cutoff $S_{co} = (f_c - f_0)^{-1/\sigma}$. The average size of an f_0 avalanche diverges as f_0 approaches f_c as

$$\langle S \rangle \sim (f_c - f_0)^{-\gamma} . \tag{12}$$

Simple integration of the power law (11) gives the usual expression for γ in terms of τ and σ, as occurs, for example, in ordinary percolation [14,63]:

$$\langle S \rangle = \int SP(S, f_0) dS; \quad \gamma = \frac{2 - \tau}{\sigma} . \tag{13}$$

A. The Bak-Sneppen branching process

Unlike the other extremal models, the evolution model has an additional feature greatly simplifying numerical studies of f_0 avalanches. The propagation of an f_0 avalanche in the evolution model is totally independent of the environment (the values of $f_i > f_0$), where it propagates. This means that, with respect to an f_0 avalanche, all of the sites with $f_i > f_0$ can be treated as vacuum sites. Sites are unimportant as long as they are not occupied by the "particles" of the f_0 avalanche. In order to study f_0 avalanches we have to keep track only of sites that have random numbers $f_i < f_0$. In simulations of this Bak-Sneppen (BS) branching process [37], which is *exactly* equivalent to an f_0 avalanche in the evolution model, we first create $2d + 1$ random numbers, chosen from the flat distribution $\mathcal{P}$, at the center of the lattice and its $2d$ nearest neighbors. Random numbers smaller than the parameter of the simulation, f_0, are stored along with their positions. At each time step, the minimal of the stored random numbers is "activated" until there are no more stored random numbers. At this point the f_0 avalanche is finished. This method gives an efficient way to study the f_0 avalanche distribution and other properties, completely free from system size corrections. An avalanche is considered infinite, and not included in the distribution, if its size is larger than a numerically imposed cutoff s_{max}, which can be made arbitrarily large. Results for the exponent τ from simulations of the BS branching process are shown for one and two dimensions in Fig. 6.

The equivalence of the off-critical BS branching process at a given value of f_0 with an f_0 avalanche in the stationary state of the evolution model also proves that f_0 avalanches in the stationary state of the evolution model have the same statistical properties as the $G = f_0$ avalanches during the transient; in particular, they have the same probability distributions. The gap equation (2) maps the transient, self-organizing behavior at a given value of the gap, G, to the stationary $f_0 = G$ avalanche distribution. We emphasize, again, that the γ for the stationary distribution in the evolution model, if it exists (i.e., if the scaling ansatz is valid), is the same γ that enters into the solution of the gap equation for the transient behavior of the model.

For the other models, we propose analogously that the $G = f_0$ avalanches during the transient also have the same scaling properties as the f_0 avalanches in the stationary state. The picture is that the scaling behavior of f_0 avalanches is not affected by correlations at distances larger than the correlation length $\xi \sim (f_c - f_0)^{-\nu}$ set by f_0. When the self-organizing system reaches a gap $G = f_0$, it has organized itself up to a scale $\xi(f_0)$; at length scales smaller than this scale, it behaves as a critical system. Thus the exponent γ that appears in Eqs. (12) and (13) is the same γ that enters into the transient approach to the critical attractor, Eqs. (3)–(5).

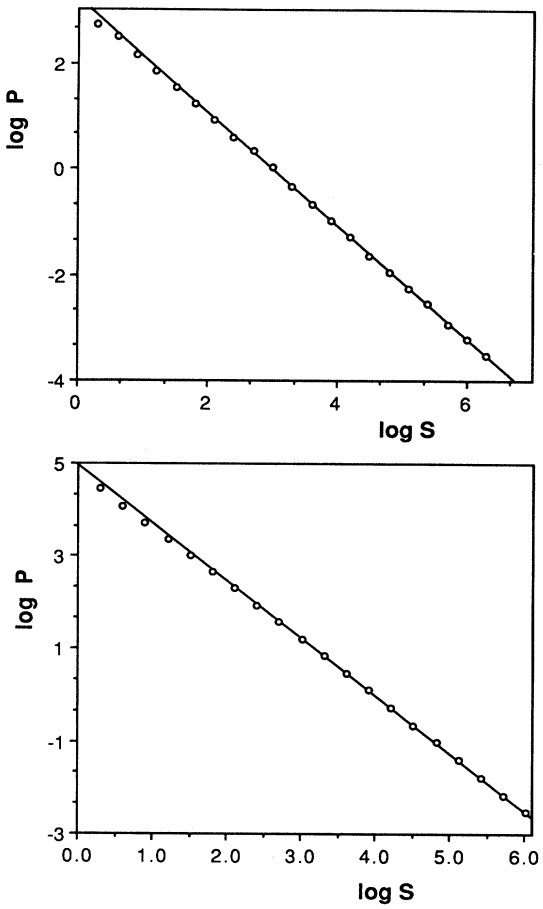

FIG. 6. Distribution of avalanches from simulation of the BS branching process in (a) one (1D) and (b) two dimensions (2D). The asymptotic slope of the log-log plot gives $\tau = 1.07 \pm 0.01$ in 1D and $\tau = 1.245 \pm 0.01$ in 2D. All logarithms (log) are base 10.

B. The "γ" equation

We now proceed to establish a general relation for the number of sites covered by an avalanche as the critical state is approached. The relation is exact for the Sneppen and evolution models, and a similar exact relation holds for IP. It leads directly to a scaling relation between the exponents τ and γ valid for all extremal models. This scaling relation was previously derived for separate mod-

els in [38,55,59,65,66]. We will reproduce here in more detail the method of derivation used in [38], which gives not only the scaling relation but the exact values of coefficients in it. The following argument applies specifically to the evolution and Sneppen models; we then generalize it to the other models.

Suppose that a value for the parameter $f_0 < f_c$ has been chosen. The moments in time, s, when the global minimal number $f_{min}(s)$ exceeds f_0 serve as breaking points dividing the temporal axis into a series of f_0 avalanches, following one after another. The probability that at any given moment the signal $f_{min}(s)$ will be greater than f_0 is given by

$$p(f_{min} > f_0) = 1/\langle S\rangle_{f_0} \quad \text{for} \quad f_0 < f_c \ , \tag{14}$$

where $\langle S\rangle_{f_0}$ is the average size of an f_0 avalanche.

Let n_{cov} denote the number of sites covered by an avalanche. These sites had their random number changed at least once during the course of the avalanche. Since each site can be updated more than once, n_{cov} is *a priori* different from the avalanche size S. In fact, for any avalanche

$$n_{cov} \leq AS \ , \tag{15}$$

where A is a constant which depends on dimension.

We can relate the divergences of these two physical quantities as the critical state is approached. This is accomplished by noting that, at the moment in time when an f_0 avalanche is finished, the random numbers at all n_{cov} sites covered by the avalanche are uncorrelated and uniformly distributed in the interval $[f_0,1]$. This is because at the last update for each site within the avalanche the random number was chosen from an uncorrelated, uniform distribution between [0,1] with the condition that it be larger than f_0. We will make repeated use of this fact in what follows.

Recall that when the f_0 avalanche started, the smallest random number in the system was larger than f_0. For simplicity, assume that this number was also larger than $f_0 + df_0$, where df_0 will be taken to be vanishingly small. When the f_0 avalanche finishes, each of the n_{cov} sites has equal probability $\frac{df_0}{1-f_0}$ to fall within the interval df_0 above f_0. Therefore $n_{cov}\frac{df_0}{1-f_0}$ is the probability that at least one of the n_{cov} sites left behind by the f_0 avalanche has a random number between f_0 and $f_0 + df_0$. If now the auxiliary parameter f_0 is raised by an infinitesimally small amount df_0, the breaking points that had $f_{min}(s)$ between f_0 and $f_0 + df_0$ will no longer stop the $f_0 + df_0$ avalanches, and the average avalanche size will increase. This property of the avalanche hierarchy is demonstrated in Fig. 7. Consider a very long temporal sequence $f_{min}(s)$ which is also a sequence of N f_0 avalanches. Increasing the auxiliary parameter to $f_0 + df_0$, the number N will be changed by $dN = -N\langle n_{cov}\rangle\frac{df_0}{1-f_0}$, to leading order in df_0 for $N \to \infty$. Of course, the sum of the temporal durations of these avalanches will remain constant. This leads to the following differential equation for the average size of an avalanche:

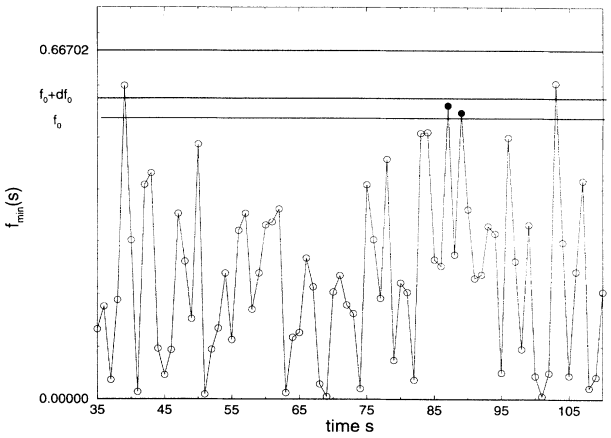

FIG. 7. One realization of the extremal signal f_{min} as a function of s in the stationary state. If the auxiliary parameter f_0 is raised by an infinitesimally small amount df_0, the breaking points that had $f_{min}(s)$ between f_0 and $f_0 + df_0$ (filled circles) will no longer stop the $f_0 + df_0$ avalanches, and the average avalanche size will increase.

$$\frac{d\ln\langle S\rangle_{f_0}}{df_0} = \frac{\langle n_{cov}\rangle_{f_0}}{1-f_0} \ . \tag{16}$$

This equation is *exact* for the evolution and Sneppen models in any dimension. It does not require the use of any scaling assumptions.

In order to proceed further, we will now assume that the avalanche distribution obeys the scaling ansatz, Eq. (11). Then for f_0 close to the critical value f_c, the average size of the avalanche diverges as $(f_c - f_0)^{-\gamma}$ [Eq. (12)]. Substituting this power law into Eq. (16) gives

$$\gamma = \lim_{f_0 \to f_c} \frac{\langle n_{cov}\rangle_{f_0}(f_c - f_0)}{1-f_0} \ . \tag{17}$$

If the critical exponent γ exists, then Eq. (17) is also exact. Note that the quantity γ appears as a constant rather than a critical exponent. It represents the average number of random numbers between f_0 and f_c left behind by an f_0 avalanche that has died, in the limit that $f_0 \to f_c$. This number is universal. For example, it does not depend on whether one updates just nearest neighbors or also includes next nearest neighbors.

A plot of $(1-f_0)/\langle n_{cov}\rangle_{f_0}$. for different values of f_0, as shown in Fig. 8 for the two-dimensional evolution model, gives f_c as the intersection with the horizontal axis, and $1/\gamma$ as the asymptotic slope close to f_c. This enables us to determine f_c very accurately, because the uncertainty in the measurement of $\langle n_{cov}\rangle$ and γ leads to an uncertainty not in f_c but in Δf. Choosing a value of f_0 near the critical point, $\Delta f = f_c - f_0$ is estimated from Eq. (17). Specifically, in the one-dimensional evolution model we choose $f_0 = 0.665$ and measure the average number of covered sites $\langle n_{cov}\rangle_{0.665} = 446.9 \pm 7.0$. Using this method for the evolution model, we find $f_c = 0.667\,02 \pm 0.000\,03$ for $d = 1$ and $f_c = 0.328\,855 \pm 0.000\,004$ for $d = 2$. Our one-dimensional result agrees with Grassberger [41]. As

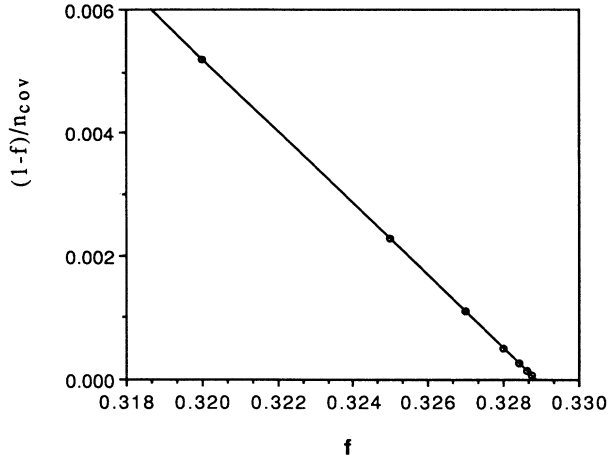

FIG. 8. The γ plot $(1 - f_0)/\langle n_{cov}\rangle$ vs f_0 for the two-dimensional evolution model. The intersection with the horizontal axis gives f_c, and the slope gives $1/\gamma$. We find $f_c = 0.328\,855 \pm 0.000\,004$ and $\gamma = 1.70 \pm 0.01$.

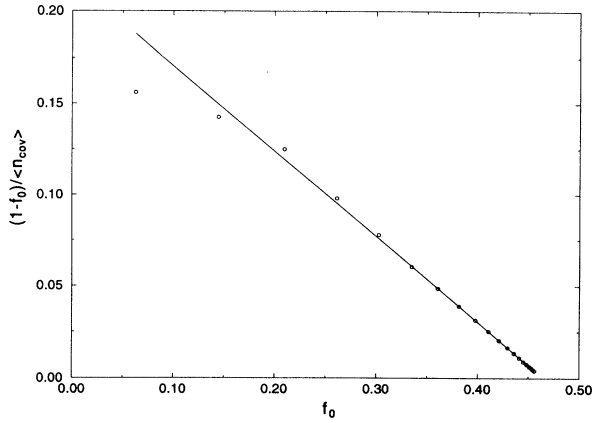

FIG. 10. The plot of $(1 - f_o)/\langle n_{cov}\rangle_{f_o}$ as a function of f_o for the one-dimensional Sneppen model. The slope of the straight line is $1/\gamma = 0.470$ and the crossing point with the f_o axis corresponds to $f_c = 0.465$.

a by-product, the one-dimensional result rules out the early speculation that f_c is exactly $2/3$ in one dimension. The exponent γ can also be estimated accurately from points further away from f_c.

Figures 9 and 10 show the same plots for the one-dimensional evolution model and the one-dimensional Sneppen model. For the one-dimensional evolution model, our result, $\gamma = 2.70 \pm 0.01$, agrees with those of Jovanovic *et al.* who measured $\gamma = 2.7 \pm 0.1$ [42] and Grassberger, who also measured 2.71 ± 0.03 [41].

For the one-dimensional Sneppen model with $L = 10^4$, we find $f_c = 0.465$ and $\gamma \simeq 2.13$. This value differs substantially from that obtained by Sneppen, $\gamma = 2.05 \pm 0.01$ at $f_c = 0.461\,36 \pm 0.000\,05$ at a system size $L = 5 \times 10^5$ [67]. Our probably less accurate result is due to finite size effects. This value $f_c = 0.465$ for the Sneppen model also does not agree with the value of $f_c = 0.4614$ that we determine from the avalanche distribution (see Sec. IV D) for a larger system size $L = 2 \times 10^5$.

For the evolution model, the value of f_c obtained using the current method, based on the "γ" equation, is used as input to determine γ from the divergence of the average avalanche size, as f_0 approaches f_c, Eq. (13). Our results for γ for the evolution model using this conventional method (this was the method used in Refs. [42] and [41]) are shown in Figs. 11 and 12. The two different methods we used to measure γ give consistent results for the evolution model. Having measured γ, we can calculate the exponent ρ for the relaxation to the critical state [Eq. (4)]. We find $\rho = 1/(\gamma - 1) = 0.588 \pm 0.004$ and $\rho = 1.43 \pm 0.01$ in the one- and two-dimensional evolution models, respectively.

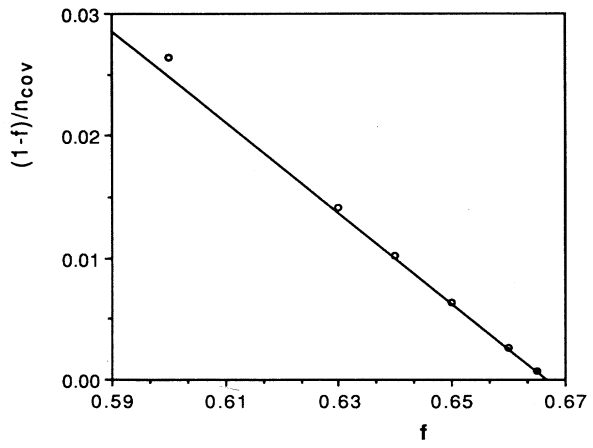

FIG. 9. As Fig. 8 for the 1D evolution model. We find $f_c = 0.667\,02 \pm 0.000\,03$ and $\gamma = 2.70 \pm 0.01$.

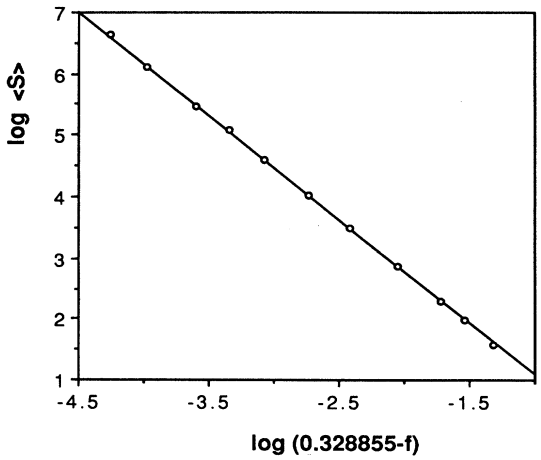

FIG. 11. The average size of avalanches $\langle S\rangle$ vs $(f_c - f)$ for the 2D evolution model. The asymptotic slope yields $\gamma = 1.69 \pm 0.03$.

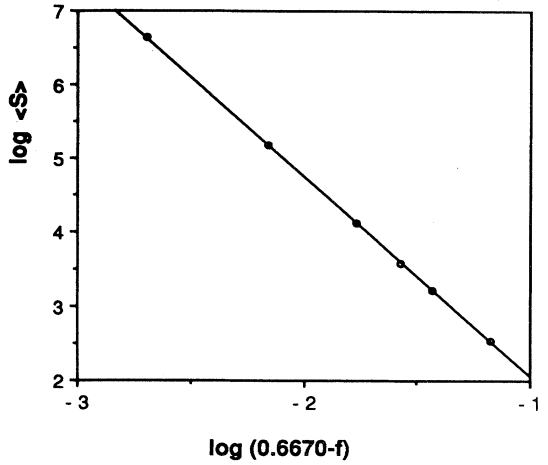

FIG. 12. The average size of avalanches $\langle S \rangle$ vs $(f_c - f)$ for the 1D evolution model. The asymptotic slope yields $\gamma = 2.71 \pm 0.02$.

The scaling form Eq. (11) for the divergence of the average avalanche size can be substituted into Eq. (14), which becomes $p(f_{min} > f_0) \sim (f_c - f_0)^{\gamma}$, or alternatively

$$p(f_{min} = f_0) \sim (f_c - f_0)^{\gamma - 1} . \tag{18}$$

From Eq. (17) it follows that the average number of sites $\langle n_{cov} \rangle_{f_0}$ covered by an f_0 avalanche scales near the critical point as

$$\langle n_{cov} \rangle_{f_0} \sim (f_c - f_0)^{-1} . \tag{19}$$

Since Eq. (15) holds for any avalanche, it is immediately clear that $\gamma \geq 1$ for any model which obeys Eq. (19). This confirms *a posteriori* that Eqs. (4) and (6) are the only allowed possibilities for the approach to the critical attractor via the gap equation. The case $\gamma < 1$ is not physically realized by the models considered here.

We are now in a position to consider the spatial extent of avalanches. Since the interactions are via nearest neighbor, it is clear that all sites visited by an avalanche form a connected cluster. In one dimension any connected cluster is also compact. Therefore in any one-dimensional model $n_{cov} \sim R_{cov}$, where R_{cov} is the length of the spatial interval formed by covered sites.

In analogy with percolation, it is conventional to define the characteristic spatial size R of an avalanche cluster as the mean square root deviation of the set of all active sites in the avalanche from their center of mass. In this definition each site is counted with the weight given by the number of times it was visited by the avalanche. The avalanche mass dimension D is defined by the scaling relation

$$S \sim R^D , \tag{20}$$

connecting the avalanche size S (temporal duration) to its spatial extent R. In the case of a *compact* d-dimensional set of covered sites, we can use another definition of the avalanche spatial size:

$$R_{cov} = n_{cov}^{1/d} . \tag{21}$$

Assuming the absence of multifractal spatial scaling behavior for avalanches implies that

$$R_{cov} \sim R . \tag{22}$$

In all extremal models that we have studied numerically thus far (excluding IP which is discussed at the end of this section), the avalanche mass dimension D was measured to be larger than the dimension of space d, and the spatial projection of all active sites within the avalanche was observed to form a compact object of dimensionality d. In what follows, we assume this is true for every extremal model below its upper critical dimension. Above the upper critical dimension (provided that it exists) the fractal dimension of the collection of covered sites is given by its mean field value d_{uc}, and can no longer form a compact object in the space of dimensionality $d > d_{uc}$. Thus in all of the scaling relations that include dimensionality, derived below and summarized in Table I, d should be replaced with d_{uc} for $d \geq d_{uc}$. This behavior is somewhat analogous to hyperscaling relations in equilibrium critical phenomena.

In the case of compact avalanches [68], $n_{cov} = R_{cov}^d \sim R^d \sim S^{d/D}$ and from Eq. (17) it follows that $(\Delta f)^{-1} \sim \langle n_{cov} \rangle \sim \int_1^{\Delta f^{-1/\sigma}} S^{d/D} S^{-\tau} dS \sim \Delta f^{(\tau - d/D - 1)/\sigma}$. As a result,

$$\sigma = 1 + d/D - \tau , \tag{23}$$

$$\gamma = \frac{(2 - \tau)}{(1 + d/D - \tau)} . \tag{24}$$

The spatial correlation length exponent ν describes the scaling of the cutoff in the spatial extent of the avalanches, $r_{co} \sim \Delta f^{-\nu}$. Since $s_{co} \sim r_{co}^D$,

$$\nu = 1/\sigma D = 1/(D + d - D\tau) . \tag{25}$$

It is interesting to observe that Eqs. (23)–(25) imply that the self-organization time to reach the critical attractor is independent of the initial state of the system, for almost any initial condition. A system of size L reaches the stationary state when $[\Delta f(s)]^{-\nu} \sim L$. The time s_{org} required for this scales as $s_{org} \sim L^{\tilde{D}}$, where $\tilde{D} = d + \frac{\gamma - 1}{\nu}$ [Eq. (5)]. Substitution of Eqs. (23)–(25) into this expression for $\tilde{D}$ gives the very simple result $s_{org} = L^D$ or $\tilde{D} = D$. Instead of starting with the initial condition where the random numbers are uniformly distributed in the interval [0,1], as assumed in the gap equation [Eq. (2)], we may start the organization process in a state where all f's are set equal to 1 except one site which has the value of f equal to, say, 0.99. In this case, none of the original 1's are ever selected as the minimal site. The organization process is finished at the moment when the last 1 is destroyed. This clearly takes $\sim L^D$ time steps, the same as for the transient that is governed by the gap equation.

We checked these scaling relations numerically. Figures 13(a) and 14 show measurements of the avalanche

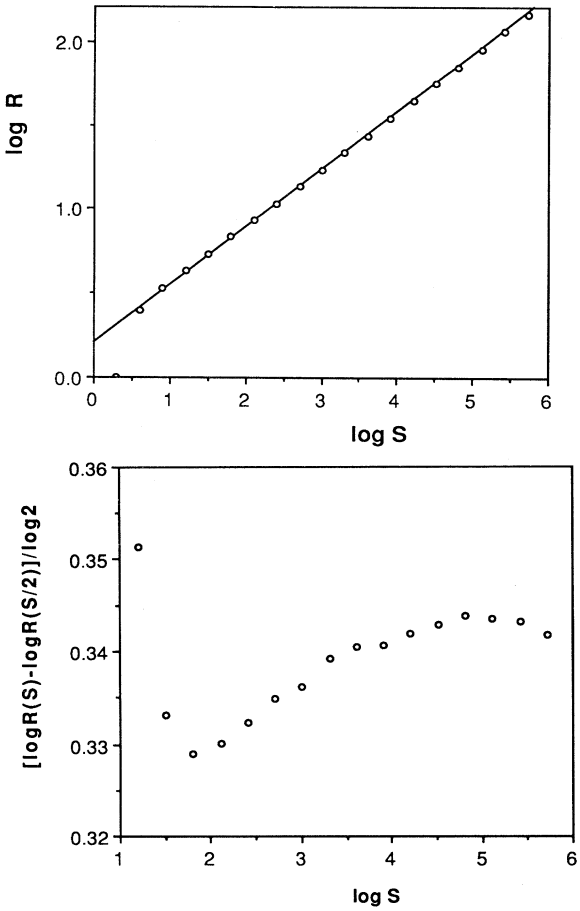

FIG. 13. (a) R vs S for the 2D evolution model (averaged over 107 000 avalanches). (b) Derivative of this curve. The asymptotic value corresponds to $1/D$ and gives $D = 2.92 \pm 0.02$.

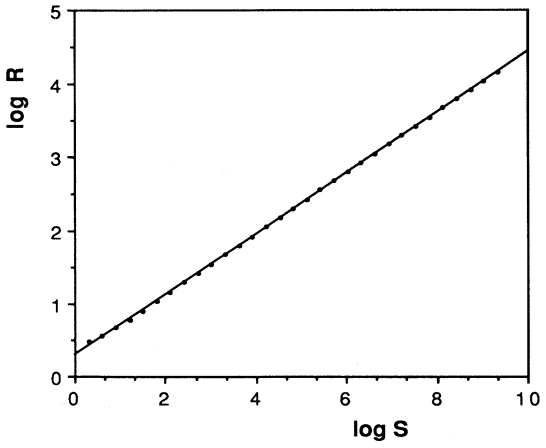

FIG. 14. R vs S for the 1D evolution model involving 3×10^{11} updates. From these data we extract $D = 2.43 \pm 0.01$.

dimension D for the one- and two-dimensional evolution models. At the critical point f_c, R_{cov} was measured as a function of S for running avalanches and their subavalanches in the BS branching process, and averaged over more than 10^{11} updates. In $d = 1$, $D = 2.43 \pm 0.01$, and in $d = 2$, $D = 2.92 \pm 0.02$. These values are consistent with the scaling relation Eq. (24) and our measured values for τ and γ. In fact, Jovanovic *et al.* [42] measured the exponent for the divergence of the average spatial size of the avalanche to be 0.98 ± 0.03 ($\tilde{\nu}_\perp$ in their notation) for the one-dimensional evolution model. Taking into account that in one dimension the spatial size is simply proportional to n_{cov} this result is consistent with the exact value of 1 we predict. In one dimension, Eq. (25) can be written as

$$\tau - 1 = \sigma\nu - \sigma \ . \tag{26}$$

For the one-dimensional evolution model, the results from Ref. [42], $\tau = 1.08 \pm 0.05$, $\sigma = 0.35 \pm 0.02$, and $1/D = \sigma\nu = 0.43 \pm 0.01$, are consistent with this last relation. Similarly, Grassberger's results $\tau = 1.073 \pm 0.003$, $\sigma = 0.343 \pm 0.004$, and $1/D = \sigma\nu = 0.4114 \pm 0.002$ [41] are also consistent with Eq. (26).

This agreement occurs in spite of the fact that it is very difficult to determine the true asymptotic value of $D = 1/(\sigma\nu)$. One reason is that the apparent exponent may be nonmonotonic, as demonstrated in Fig. 13(b). The effective exponent as plotted here is measured by numerically calculating the local slope of the curve R vs S. It is apparent for the two-dimensional model that the effective exponent $\sigma\nu = 1/D$ does not approach its asymptotic value monotonically but first overshoots with a maximum around $S \simeq 10$ and then undershoots with a minimum around $S \simeq 10^2$. There are indications that similar behavior may occur in the one-dimensional model at much larger avalanche scales. Our numerical capability for the one-dimensional model is not sufficient to be sure that we are observing asymptotic behavior despite studying 3×10^{11} time steps, and thus 3×10^{11} avalanches and subavalanches. In addition, simulations of the related $M \to \infty$ evolution model [53], where $D = 4$ is known exactly, indicate that there are large corrections to scaling for R_{cov}. Thus the numerical studies thus far have not conclusively refuted the conjecture [37,38], based on symmetry arguments, that the exponents D and τ in the evolution model are the same as directed percolation, or Reggeon field theory. It seems dangerous to us to base conclusions about universality on differences of less than 2% in the observed "asymptotic" regime at $S \simeq 10^6$ [41] in one dimension. In two dimensions, the disagreement is within error bars and less than 1%.

Equation (16) can be generalized to include IP with the following consideration. In IP the list of growth sites from which the minimal number is selected is not a compact d-dimensional lattice of linear size L, but the fluctuating fractal boundary of the invaded cluster. Comparing the list of potential growth sites before and after an f_o avalanche, one observes that some sites were invaded during this specific avalanche and thereby removed from the list. In addition, the result of an f_0 avalanche in IP-2

and IP-3 may be a new internal "lake" in the invading cluster, so sites on the lake perimeter are now excluded from the active boundary as well (see the Appendix). On the other hand, some new boundary sites may have been added. We will denote this latter number of *new* boundary sites added by an avalanche of size R as $n_{new}(R)$. Since these sites constitute a part of the active boundary of the region invaded by the avalanche, it is reasonable to assume that

$$n_{new}(R) \sim R^{d_B} , \tag{27}$$

where d_B is the fractal dimension of the active boundary of the invaded region. All of these new random numbers are uncorrelated and uniformly distributed between f_0 and 1. By replacing the number of covered sites n_{cov} with the number of new sites added to the boundary, n_{new}, we find that Eqs. (16) and (17) apply to IP as well.

Using Eq. (27) we can derive exponent relations analogous to Eqs. (23) and (24) for IP: $(\Delta f)^{-1} \sim \langle n_{new} \rangle_{f_0} \sim \int_1^{\Delta f^{-\nu D}} s^{d_B/D} s^{-\tau} ds \sim \Delta f^{(\tau-1-d_B/D)\nu D}$, which gives

$$\tau = 1 + \frac{d_B - 1/\nu}{D} , \tag{28}$$

$$\gamma = 1 + (D - d_B)\nu . \tag{29}$$

Although the exact equations (16) and (17), with n_{cov} replaced with n_{new}, are new for invasion percolation, the scaling relations (28) and (29) are well known. To the best of our knowledge, they were first derived by Gouyet [69]. Substitution of Eqs. (29) and (8) into Eq. (10) simplifies the final form of the transient approach to the critical state for IP:

$$\Delta f \sim (s/L^d)^{-\frac{1-g}{\gamma-1}} \sim (s/L^d)^{-\frac{1-g}{\nu(D-d_B)}} \sim (s/L^d)^{-\frac{1}{\nu(D-d)}} . \tag{30}$$

The time required to complete self-organization $s_{org} \sim L^{d+\frac{\gamma-1}{\nu(1-g)}} \sim L^D$. Equation (30) agrees with results from [35] obtained using different arguments.

Equation (14) holds for any extremal model where $f_{min}(s)$ has a well defined threshold level f_c in the thermodynamic limit. At the same time, though, Eqs. (16) and (17) are not valid for the Zaitsev model and LIM. The reason is that for these two models the distribution of internal forces left by an f_0 avalanche is not flat and uniform in the interval $[f_0, 1]$. However, as long as this distribution is not singular in the limit that $f_0 \to f_c$, and these internal forces are uncorrelated, as is reasonable to assume, the result $\langle n_{cov} \rangle \sim (f_c - f_0)^{-1}$ still holds, and, therefore, the scaling relations (23)–(25) are valid. For interface models, it is customary to express scaling relations in terms of D and ν as basic exponents. Our scaling relations will then read

$$\tau = 1 + \frac{d - 1/\nu}{D} , \tag{31}$$

$$\gamma = 1 + (D - d)\nu . \tag{32}$$

C. Law for stationary states: $\eta = 0$

In this section we derive a law for the activity in the stationary state for the class of SOC extremal models defined in Sec. II. Recall that an f_c avalanche starts when *all* sites in the system have random numbers, or internal forces, above the threshold f_c. In the following discussion, we will only consider f_c avalanches, and therefore drop the label f_c. During the course of the avalanche there will be sites denoted as *active* sites, or "particles," where the random numbers f_i are less than the threshold f_c. The number of these active sites after s updates is denoted the "activity" $n(s)$. This quantity is just the number of sites in the system that have random numbers less than f_c. The current avalanche stops when all sites in the system again have random numbers above f_c, or when $n(s)$ first returns to zero. Then a new avalanche will start somewhere else in the system. The probability distribution for avalanche sizes, $P(S) \sim S^{-\tau}$, is therefore, by definition, also the probability distribution of interval lengths between subsequent returns of $n(s)$ to zero.

Figure 15 shows a typical $n(s)$. The collection of return points, $\{n(s) = 0\}$, forms a fractal with dimension $\tilde{d} = \tau - 1$ on the one-dimensional time line. This relationship for $\tilde{d}$ is explained in the next section [see Eq. (50)]. As long as $\tilde{d} < 1$, the threshold f_c is well defined in the thermodynamic $L \to \infty$ limit. The initiation of a new avalanche in the stationary state can be viewed as the injection of a single "particle" into the system. Thus the average number of return points, or number of injected particles, added in an interval of s steps is $n_{INJ} \sim s^{\tilde{d}}$.

We examine the average number of active sites S steps after a *single* particle has been injected into the system, $\langle n(S) \rangle \sim S^{\eta}$. This quantity is by definition the average activity $n_{SURV}(S) \sim S^{d_s}$ of the avalanches that survive S steps multiplied by the probability of survival, $P(s' > S) \sim S^{1-\tau}$. Avalanches that die out before S steps are counted with *zero* particles in the average $\langle n(S) \rangle$, while the surviving avalanches are counted with their actual number of active sites $n(S)$. The quantity $n_{SURV}(S)$ is

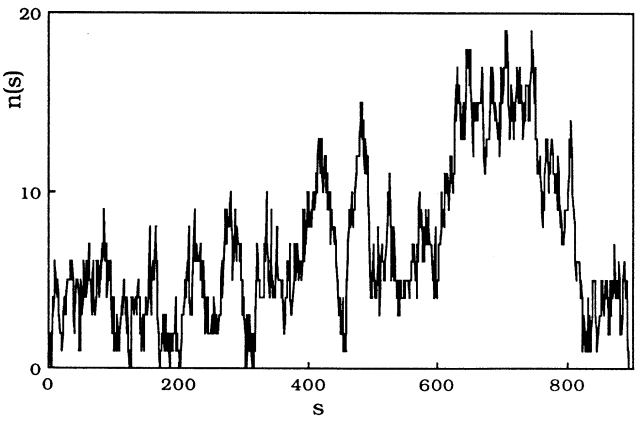

FIG. 15. Typical $n(s)$ for the two-dimensional evolution model.

an average over avalanches that survive S steps, while $\langle n(S)\rangle$ is an average over *all* avalanches, hence the factor $P(s' > S)$. We now utilize the hierarchical nature of the stationary process: we propose that the activity of the large avalanches after S steps scales in the same way as the amount of activity injected into the system during a time interval of length S:

$$n_{SURV}(S) \sim n_{INJ}(S) \ , \quad \text{or } d_s = \tilde{d} = \tau - 1 \ . \tag{33}$$

That is, there is only one dimension for the activity in the critical process. Thus

$$\begin{aligned} \langle n(S)\rangle &\equiv n_{SURV}(S)\ P(s' > S) \\ &\sim n_{INJ}(S) S^{1-\tau} \sim S^0 \ , \text{ i.e., } \ \eta = 0 \ . \end{aligned} \tag{34}$$

In order to illustrate the argument by an elementary example, consider a simple, uncorrelated one-dimensional random walk, with the activity increasing or decreasing by 1 with equal probability at each step. This is the mean field, SOC state in many models [50–52]. The infinite random walk can be viewed as a sequence of avalanches. These avalanches are, by definition, the intervals between subsequent returns of the walk to zero. The exponent τ for the first return times is $\tau = 3/2$, so the probability of s' exceeding S scales as $S^{-1/2}$. The average number of returns in S steps, $n_{INJ}(S) \sim S^{1/2}$, scales in the same way as the activity of surviving avalanches after S steps, $n_{SURV}(S) \sim S^{1/2}$. Thus the average activity after S steps of a single avalanche is $\langle n(S)\rangle \sim S^{1/2} S^{-1/2} \sim S^0$, and $\eta = 0$ rigorously.

Figure 16 shows the average activity of a single avalanche, $\langle n(S)\rangle$, in the two-dimensional evolution model. The exponent η reflects the average activity S time steps after starting a single realization of the BS branching process at f_c. The quantity $\langle n(S)\rangle$ saturates for large S, varying only 2% over *four decades*; this is consistent with $\eta = 0 \pm 0.002$ in two dimensions. Figure 16 is our strongest numerical confirmation of the $\eta = 0$ prediction. As alluded to earlier, in one dimension there are larger corrections to scaling and the saturation regime obtained numerically is smaller, although the overall behavior is the same, as shown in Fig. 17. The slope is decreasing and reaches $\eta = 0.01 \pm 0.02$ at $s = 6 \times 10^7$.

The fractal dimension of active sites within a surviving avalanche is defined by the relation $n_{SURV}(r) \sim r^{d_f}$, where r is the spatial extension of the avalanche cluster. Using the relation $s \sim r^D$ and Eq. (33), we find the relation

$$d_f = D d_s = D(\tau - 1) \ , \tag{35}$$

connecting the geometrical properties of the active sites to the properties of the entire avalanche clusters. Figure 16 (17) also shows $n_{SURV}(S)$ vs S in two (one) dimensions for the evolution model. At the largest time scales measured, the slope of the curves yields $d_s = 0.11 \pm 0.02$ and $d_s = 0.25 \pm 0.005$ in one and two dimensions. In two dimensions, this is consistent with our measured value of $\tau - 1$ (cf. Fig. 7), but in one dimension our measured value of $\tau - 1$ is somewhat lower. This is probably a consequence of the slow convergence of the slope, as is evident from Fig. 17. Actually, Grassberger measured $n_{SURV}(S) \sim S^{0.74}$ for the one-dimensional evolution model, which agrees with his measured value for τ [41], and thus with Eq. (33) and $\eta = 0$.

The usual dynamical exponent relating space and time, z, where $t \sim r^z \sim s^{z/D}$, can also be measured. The parallel time unit t is different from the sequential time unit s. It is defined as the average number of update steps for changing all active sites, so that time increases by an amount $1/n(s)$ at each update, i.e., $s \to s + 1$, $t \to t + 1/n(t)$. It appears naturally in models for depinning at constant force, for example, because all unstable

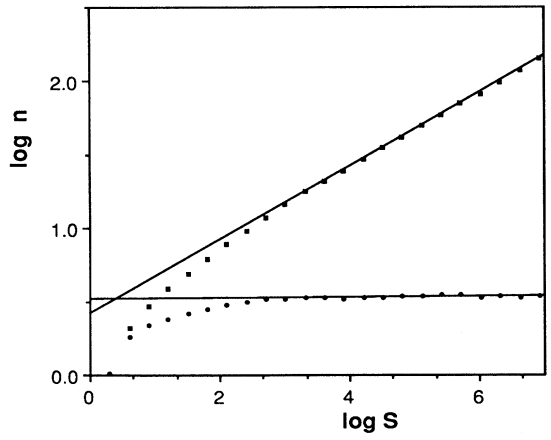

FIG. 16. Average number of active sites $\langle n(S)\rangle$ vs S (lower curve) and average activity of surviving avalanches, $n_{SURV}(S)$, (upper curve) for the two-dimensional evolution model at $f_c = 0.3289$. The slopes yield $d_s = 0.25 \pm 0.005$ and $\eta = 0.0 \pm 0.002$, respectively.

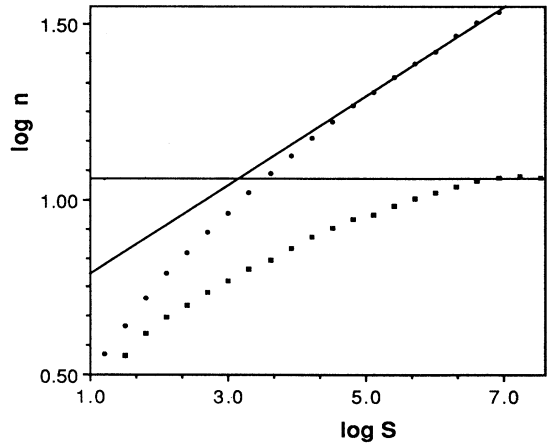

FIG. 17. Average number of active sites $\langle n(S)\rangle$ and average activity of surviving avalanches, $n_{SURV}(s)$, for the one-dimensional evolution model at $f_c = 0.6670$. The slopes yield $d_s = 0.11 \pm 0.02$ and $\eta = 0.01 \pm 0.02$.

sites move together. We introduce the dynamical exponent z also for the sequential models in order to compare dynamical critical behavior in the different situations.

For this definition of time, clearly $s \sim nt$ and $d_s + z/D = 1$. Within the superuniversal class where $\eta = 0$, including the extremal SOC models discussed here, the exponent z is given by the scaling relation

$$z = D - d_f = D(2 - \tau) \ . \tag{36}$$

We measured the dynamical exponent $z = 1.19 \pm 0.05$ for the Sneppen model in one dimension as shown in Fig. 18. This value is close to the theoretically predicted value $z = 1.21$, obtained by using Eq. (36) with $D = 1.63$ [55], and our measured value of τ. We have also measured the dynamical exponent z for the one- and two-dimensional evolution models as shown in Fig. 19. In two dimensions, $z = 2.16 \pm 0.02$. Inserting our measured values for τ and D into the expression for z we predict $z = 2.20 \pm 0.04$, in fairly good agreement. In one dimension we find $z = 2.26 \pm 0.05$ to be compared with the somewhat lower measured value 2.10 ± 0.05. This discrepancy again may reflect slow convergence for the one-dimensional evolution model. Jovanovic *et al.* [42] measured a dynamical exponent (in their notation $\nu_{\|}/\nu_{\perp}$) $= 2.1 \pm 0.1$ for the one-dimensional evolution model using the tree structure of the avalanches. The dynamical exponent that they measured may be equivalent to our definition of z, and their result is consistent with our prediction, again within numerical uncertainty.

An alternative way of deriving $\eta = 0$ follows. Consider either the evolution or Sneppen model in the stationary state, and select an arbitrary value f_0 below f_c. We focus on the number of active sites with random numbers below f_c. As explained in the preceding subsection, when an f_0 avalanche ends, it leaves behind uncorrelated random numbers uniformly distributed between f_0 and 1. As a result, the average number of active sites

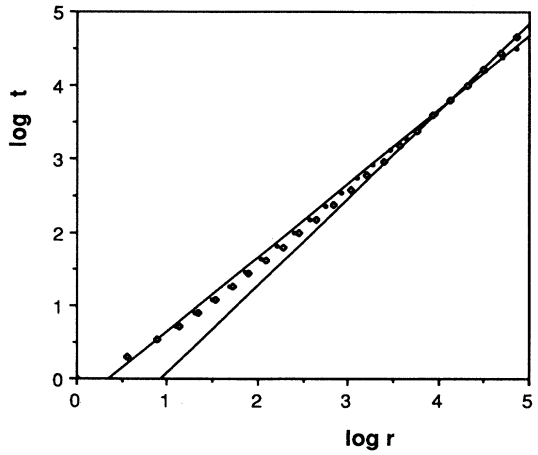

FIG. 18. Parallel time t vs spatial extension r for the one-dimensional Sneppen model (open dots) and the one-dimensional TLB model (filled dots). The slopes give $z = 1.19 \pm 0.05$ for the Sneppen model and $z = 1.00 \pm 0.05$ for the TLB model.

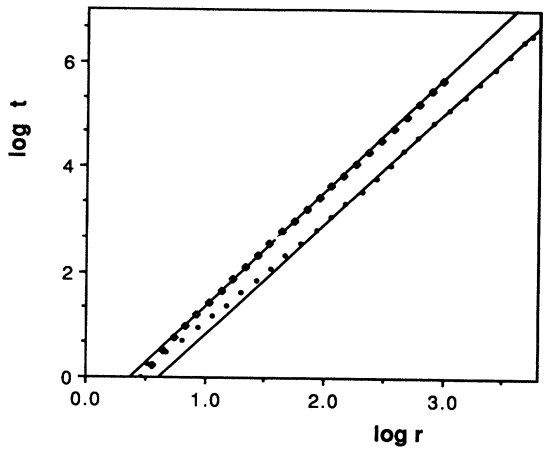

FIG. 19. Parallel time t vs spatial extension r for the two-dimensional (small filled dots) and one-dimensional evolution (large open dots) models. The asymptotic slopes are $z = 2.17 \pm 0.02$ and $z = 2.10 \pm 0.05$, respectively.

created, or left behind, by an f_0 avalanche is exactly $\langle n_{cov} \rangle_{f_0} (f_c - f_0)/(1 - f_0)$ [see Eq. (17)]. We assume that when the f_0 avalanche started the active sites between f_0 and f_c were distributed on a fractal, with dimension d_f. As a result, the average number of actives sites that are destroyed by the f_0 avalanche scales as $\langle R^{d_f} \rangle_{f_0}$, where R is the spatial extension of the avalanche. In the stationary, critical state the average number of active sites created and destroyed by an f_0 avalanche must be equal. Assuming a power law distribution of avalanche sizes with cutoff $R_{co} \sim (f_c - f_0)^{-\nu}$, we find

$$1 = \nu(d - d_f) \ . \tag{37}$$

Using the scaling relation, $\tau = 1 + (d - 1/\nu)/D$ [Eq. (25)] we again obtain our fundamental result $\eta = d_f/D - \tau + 1 = 0$. Equation (37) is reminiscent of the hyperscaling relation $\beta = \nu(d - d_f)$ valid for equilibrium systems, and for directed percolation [70].

In order to take this alternative argument over to the Zaitsev model and LIM, one makes the same assumption that was made for the γ equation, i.e., the distribution of internal forces left behind by an f_0 avalanche is uncorrelated and smooth. We have measured $\langle n(s) \rangle$ and $n_{SURV}(s)$ for the Zaitsev flux creep model [29] in one dimension, as shown in Fig. 20. These results are consistent with $\eta = 0$. Finally, we predict that $\eta = 0$ for invasion percolation.

Although the $\eta = 0$ law applies to a broad class of SOC phenomena, it does not generally apply to systems that are tuned to be critical, since for non-SOC systems the critical state may not be stationary. For instance, in directed percolation $\eta = d_f/D - \tau + 1 \simeq 0.21$ [71] in one dimension. Also, in directed percolation the fractal dimension of active sites obeys a hyperscaling relation $d_f = d - D(\tau - 1)$. This hyperscaling relation is inconsistent with the relation $d_f = D(\tau - 1)$ that holds for

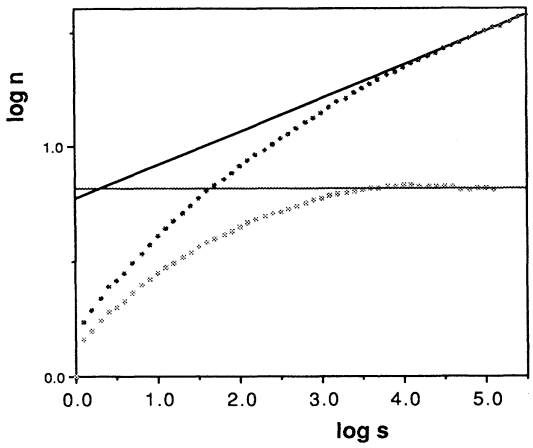

FIG. 20. $\langle n(S)\rangle$ and $n_{SURV}(S)$ for the one-dimensional Zaitsev model with $L = 10^4$. $d_s = 0.15 \pm 0.03$. The asymptotic value of the slope of $\langle n(S)\rangle$ is $\eta = 0.0 \pm 0.006$.

the extremal SOC models that we study. Thus directed percolation does not belong to the superuniversal class defined by the dimension independent law $\eta = 0$.

The models for depinning at constant force, such as the TLB model or parallel LIM, also do not in general obey $\eta = 0$, or the corollary results $d_f = D(\tau - 1)$ and $z = D(2 - \tau)$. For example, in the one-dimensional TLB model at constant force, it has been predicted and confirmed numerically that $z = 1$ [62]. Our measured value for this model $z = 1.00 \pm 0.05$, as shown in Fig. 18, is consistent with this prediction. Since $D \simeq 1.63$ and $\tau \simeq 1.26$ are the same as for the Sneppen model (see Sec. VI), one can compare with the different prediction $z \simeq 1.21$ based on the $\eta = 0$ law. Since η is not zero for the tuned depinning models at constant force, while it is zero for the SOC depinning models, the critical dynamics of a self-organizing system are different from the critical dynamics of a tuned system. Thus SOC cannot be simply viewed as sweeping an instability [43]. If the TLB model were to be studied at constant *velocity*, we predict that $\eta = 0$ and $z \simeq 1.21$, as for the SOC (Sneppen) case. Thus the dynamical critical exponents, such as z, depend on how the depinning transition is probed.

The existence of a stationary limit may imply that $\eta = 0$ for a very broad class of SOC models, beyond those studied here. In addition, Pietronero [25] and coworkers explicitly make use of the stationary limit in the fixed scale transformation method. This suggests that stationarity may potentially provide more powerful tools to understand SOC and fractal growth phenomena in a wider range of systems.

D. Backward avalanches

The dynamics of extremal models forms a hierarchical structure. We have defined f_0 avalanches as the activity between subsequent moments in time when the signal $f_{min}(s)$ is larger than an auxiliary parameter f_0. Then, as the parameter f_0 is decreased, larger avalanches are subdivided into smaller ones because new breaking points appear. For the sake of clarity in this section, we will now refer to avalanches defined by this specific rule as f_0 punctuating avalanches, since they correspond to a sequence of events between subsequent punctuations of the f_0 barrier by the signal $f_{min}(s)$. Another way of looking at the hierarchy is to define avalanches by a slightly different rule. According to the new rule, a forward avalanche begins at *every time step* s. It runs as long as $f_{min}(s + s') \leq f_{min}(s)$, and will stop at the first moment $s + S$ *forward* in time when $f_{min}(s + S) > f_{min}(s)$. This avalanche is similar to an f_0 punctuating avalanche, except that now we set f_0 exactly to the value of the signal $f_{min}(s)$ at the starting point of the avalanche. In the evolution model, the mapping to the BS branching process proves that the probability to have an f_0 punctuating avalanche of size S is *exactly* the same as the conditional probability to have a forward avalanche of this size, given that the value of the signal at the beginning of the avalanche was f_0. That is, the exact knowledge of the value of the signal $f_{min}(s) \geq f_0$ at the starting point of an f_0 avalanche does not influence its statistics. This follows from the observation that the site carrying $f_{min}(s)$ gets a new random number at the very first time step of the avalanche and all the information about its previous value is erased from the system. Therefore the conditional probability $P_f(S, f_0)$ to have a forward avalanche of size S, given that the signal at its starting point was equal to f_0, is exactly equal to the probability $P(S, f_0)$ to have an f_0 punctuating avalanche of size S. Then from Eq. (11)

$$P_f(S, f_0) = P(S, f_0) = S^{-\tau} g(S(f_c - f_0)^{1/\sigma}) \ . \quad (38)$$

For the other models we lack a rigorous proof, so we simply conjecture that both $P_f(S, f_0)$ and $P(S, f_0)$ scale [e.g., Eq. (11)] with the same exponents τ and σ, but with possibly different scaling functions $g_f(x)$ and $g(x)$. With this assumption, the results which follow in this section also apply to the other SOC extremal models.

To study the properties of the signal under time reversal it is useful to define *backward avalanches*. Now we look for the first moment *back* in time when $f_{min}(s - S) > f_{min}(s) = f_0$. The definitions of both forward and backward avalanches are illustrated in Fig. 21. This figure demonstrates the hierarchy in the avalanche structure: all forward and backward avalanches that start inside one big forward (backward) avalanche are constrained to not go beyond the limits of the parental avalanche and, therefore, can be considered to be its subavalanches. Each subavalanche in turn has its own subavalanches, and so on. One can look at the entire activity in an extremal model as one great parental critical avalanche, which began in the distant past. It contains subavalanches of all sizes.

Since all extremal processes are intrinsically irreversible, it is possible to have different statistical properties for the forward and backward avalanches. In analogy

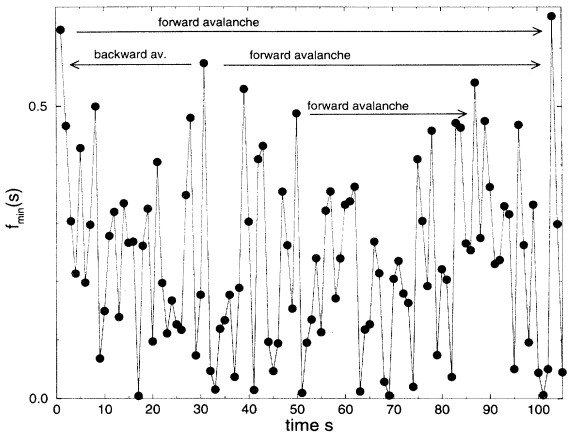

FIG. 21. The hierarchical structure of backward and forward avalanches. The avalanches that started inside a larger parental avalanche are completely contained within it.

with Eq. (38), we conjecture a scaling form for the conditional backward avalanche probability distribution:

$$P_b(S, f_0) = \frac{1}{N} S^{-\tau_b} g_b(S(f_c - f_0)^{1/\sigma}) \ , \qquad (39)$$

where $g_b(x)$ is a scaling function that rapidly decays to zero for $x \gg 1$. We will prove later that the cutoff exponent σ in this expression is the same for both forward and backward avalanches, while the power-law exponents τ_b and τ are different. In fact $\tau_b < 1$, so that a normalization factor $1/N$ must be included in the conditional probability distribution for backward avalanches.

According to Eq. (18), the minimal numbers selected at different time steps are distributed with probability density $p(f_{min} = f_0) \sim (f_c - f_0)^{\gamma - 1}$, where $\gamma = \frac{2-\tau}{\sigma}$ is the critical exponent governing the divergence of the average punctuating avalanche size. The distribution of *all* forward avalanches, $P_f^{all}(S)$, is obtained by integrating the conditional probability from Eq. (38) with the proper weight from Eq. (18) to give

$$\begin{aligned} P_f^{all}(S) &= \int_0^{f_c} P_f(S, f_0)\, p(f_{min} = f_0) df_0 \\ &= \int_0^{f_c} S^{-\tau} g(S(f_c - f_0)^{1/\sigma})\, (f_c - f_0)^{\gamma - 1}\, df_0 \\ &= S^{-\tau - \sigma\gamma} = S^{-\tau - \sigma(2-\tau)/\sigma} = S^{-2} \ . \end{aligned} \qquad (40)$$

The unexpected result is that the exponent for this distribution has the *superuniversal* value -2 in all dimensions.

For the distribution of all backward avalanches $\tau_b < 1$, and the normalization factor $1/N = 1/\int_1^\infty S^{-\tau_b} g_b(S(f_c - f_0)^{1/\sigma}) dS = (f_c - f_0)^{\frac{1-\tau_b}{\sigma}}$ enters. Integrating Eq. (39) gives

$$\begin{aligned} P_b^{all}(S) &= \int P_b(S, f_0)\, p(f_{min} = f_0)\, df_0 \\ &\sim S^{-\tau_b - \sigma(1-\tau_b)/\sigma - \sigma(2-\tau)/\sigma} = S^{\tau - 3} \ . \end{aligned} \qquad (41)$$

The exponent τ_b does not enter into the final expression for $P_b^{all}(S)$ as long as $\tau_b < 1$. The exponent for the distribution of all backward avalanches is model and dimension dependent and is related to the usual f_0 avalanche distribution exponent τ.

In numerical simulations, the exponent τ is conventionally measured from the distribution $P(S, f_0)$ of f_0 punctuating avalanches with the value of f_0 carefully chosen as close as possible to the actual threshold f_c. Since backward avalanches are defined at every time step, while $P(S, f_0)$ gets contributions only when $f_{min}(s) > f_0$, the distribution $P_b^{all}(S)$ has much better statistics than $P(S, f_0)$ after the same number of time steps. It is also very convenient that $P_b^{all}(S)$ automatically has no cutoff, so one does not need to know f_c in order to measure its power law. Thus $P_b^{all}(S)$ provides, in principle, a very accurate way to measure τ for the extremal SOC models discussed here. However, we have not yet pushed this technique to its ultimate limit.

We have measured $\tau_b^{all} = 3 - \tau$ in the one-dimensional Sneppen model, and the one- and two-dimensional LIM's. These results are shown in Figs. 22 and 23. For the Sneppen model, our numerical results from the backward avalanche distribution give $\tau = 1.255 \pm 0.02$, in agreement with the value of 1.25 ± 0.05 measured by Tang and Leshhorn [54], and $\tau = 1.26 \pm 0.01$ measured by us (Fig. 24) using the conventional method. The LIM results, $\tau_{1D} = 1.13 \pm 0.03$ and $\tau_{2D} = 1.29 \pm 0.03$, are in agreement with the results from numerical simulations on self-affine one-dimensional interfaces in porous media from [60], and two-dimensional domain walls in the random field Ising model [61]. This supports the possibility that these models might be in the universality class of the LIM; a more detailed comparison is made in Sec. VI.

A study of backward avalanches leads to an exponent relation for τ_b, and a proof that f_0 backward avalanches have the same cutoff as f_0 punctuating (or forward) avalanches. For the sake of simplicity we concentrate on the case of the evolution model, where the only as-

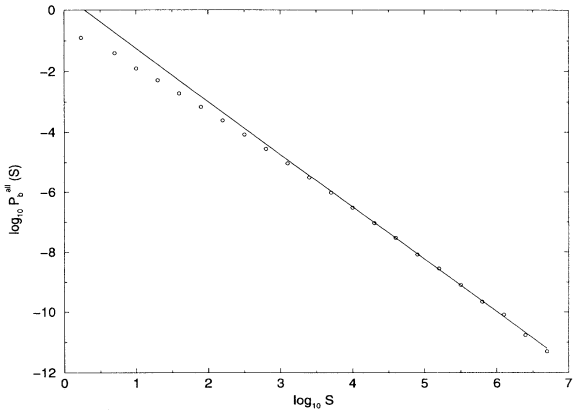

FIG. 22. The overall distribution of backward avalanches in the 1D Sneppen model. The slope of the curve gives $\tau_b^{all} = 3 - \tau = 1.745 \pm 0.02$. We simulated 10^7 time steps in a system of size $L = 1000$.

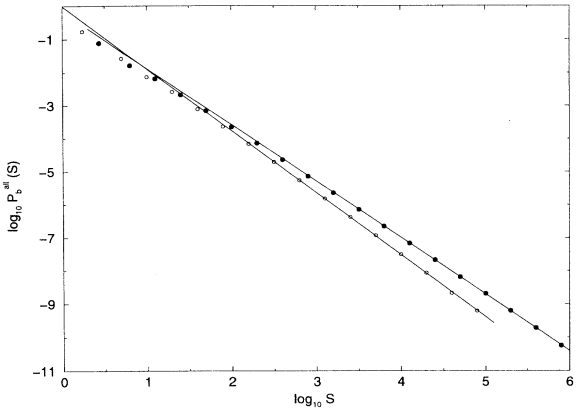

FIG. 23. The overall distribution of backward avalanches in 1D (open circles) and 2D (closed circles) LIM. In 1D, the slope of the curve corresponds to $\tau_b^{all} = 3 - \tau = 1.87$ from simulations of 5×10^7 time steps in a system of size $L = 3000$. In 2D, the slope of the curve corresponds to $\tau_b^{all} = 3 - \tau = 1.71$ from simulations of 10^9 time steps in a system of size 300×300.

sumption is that the scaling forms Eqs. (38) and (39) for the avalanche distributions exist. With the additional assumptions that have already been mentioned, the resulting scaling relations also apply to the other SOC extremal models defined in Sec. II.

Consider an arbitrary f_0 punctuating avalanche. The probability distribution $P(S, f_0)$ for the size S of this avalanche is given by Eq. (38). For this f_0 punctuating avalanche to be also a valid f_0 backward avalanche, starting at $s + S$ and running backwards in time down to s, one needs $f_{min}(s + S) = f_0$. We next calculate what fraction of f_0 punctuating avalanches are also f_0 backward avalanches. Suppose we have a temporal sequence $f_{min}(s)$ which is an ensemble of N f_0 punctuating avalanches, where N is a sufficiently large number.

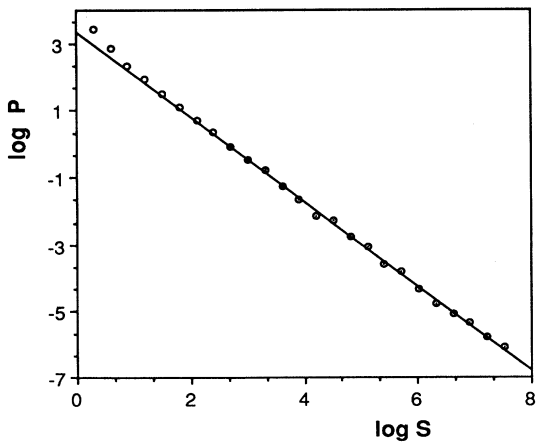

FIG. 24. Distribution of avalanches from simulations of the 1D Sneppen model for $L = 2 \times 10^5$ and $f_c = 0.4614$. The asymptotic slope of the log-log plot gives $\tau = 1.26 \pm 0.01$.

The average number of f_0 punctuating avalanches of size S in such an ensemble is given by $N(S) = NP(S, f_0)$. At the end of any f_0 avalanche of size S, n_{cov} sites have acquired new random numbers. If the avalanches are compact, then $n_{cov} \sim S^{d/D}$. All these random numbers are *uncorrelated* and uniformly distributed between f_0 and 1. To have $f_{min}(s + S) = f_0$ we need the minimal number in the system to lie between f_0 and $f_0 + df_0$. This number can be only at one of these n_{cov} updated sites, since at the beginning of the avalanche every number in the system was larger than f_0. The probability that at least one of these numbers will be between f_0 and $f_0 + df_0$ is given by $n_{cov} \frac{df_0}{1-f_0} \sim S^{d/D} \frac{df_0}{1-f_0}$. The number $N_b(S)$ of valid f_0 backward avalanches of size S in our ensemble is $N_b(S)df_0 = NP(S, f_0) n_{cov} \frac{df_0}{1-f_0} \sim NP(S, f_0) S^{d/D} \frac{df_0}{1-f_0}$. Therefore the conditional probability distribution of f_0 backward avalanches obeys

$$P_b(S, f_0) \sim S^{d/D} P(S, f_0) \ , \tag{42}$$

where the proportionality constant is determined from the normalization condition $\sum_{S=1}^{\infty} P_b(S, f_0) = 1$.

Intuitively, it is clear that larger f_0 punctuating avalanches affect a larger number of sites. These larger avalanches are more likely to leave behind a new random number between f_0 and $f_0 + df_0$ and thus constitute a valid f_0 backward avalanche. This explains why the distribution of backward avalanches acquires an additional factor of $S^{d/D}$ compared to punctuating (or forward) avalanches. Equation (42) shows that both forward and backward avalanche distributions have the same cutoff as a function of f_0, and their power-law exponents obey the relation $\tau_b = \tau - d/D$.

From Eq. (31), we get a particularly simple expression for τ_b:

$$\tau_b = 1 + \frac{d - 1/\nu}{D} - \frac{d}{D} = 1 - \frac{1}{\nu D} = 1 - \sigma \ . \tag{43}$$

Since σ must be positive, this proves that $\tau_b < 1$ and confirms *a posteriori* the validity of Eq. (41).

All equations in this section apply to IP with the dimension d replaced with d_B (see the Appendix). The importance of forward avalanches in IP was first recognized by Roux and Gouyon [35]. However, they made some erroneous assumptions which led to incorrect scaling relations. Our exponent relations agree well with their numerical results, though. For IP-2, where $d_B = 1.75$ and $D = 1.89$, they measured $\tau_b^{all} = 1.50 \pm 0.04$ which is consistent with our prediction $\tau_b^{all} = 1.47$ based on Eq. (43) and the assumption that $\nu = 4/3$ as in ordinary percolation [63].

E. Lévy flight distribution

In the stationary state, the minimal site jumps throughout the system in a correlated and anomalous fashion which has some similarity to the usual Lévy flight picture. Specifically, one can record the spatial location $\vec{r}_{min}(s)$ of the current extremal site (with the smallest random number) as a function of time s [29,31,32]. The

distribution $P_{jump}(r)$ of jumps $r = |\vec{r}_{min}(s) - \vec{r}_{min}(s-1)|$ between subsequent extremal sites follows a power law:

$$P_{jump}(r) \sim r^{-\pi} . \tag{44}$$

This behavior is reminiscent of the Lévy flight random walk (LFRW), where at every time step the walker jumps in a random direction by a distance that is drawn from a power-law distribution. In contrast to the uncorrelated LFRW, the jumps of activity in extremal models are temporally correlated, so that even if $\pi > 3$ and, therefore, the jump distribution has finite first and second moments, the process does not necessarily reduce to ordinary diffusion.

The exponent π can be related to other exponents as follows. Consider a backward avalanche that started at time step s. Suppose it has size S. By definition, $f_{min}(s-S) > f_{min}(s)$, while $f_{min}(s-k) < f_{min}(s)$ for $1 \leq k \leq S-1$. Looking at the same sequence of events forward in time from time step $s-S$ to s, one notices that the forward avalanche with $f_0 = f_{min}(s-S)$ that was started at time step $s-S$ is still running at s. At this moment s, $n_{cov} \sim S^{d/D}$ sites acquired new random numbers since time step $s-S$. The active sites at time steps s and $s-1$ are both rigorously constrained to belong to this specific set of covered sites.

Looking further back in time one may find another forward avalanche, which is still running at time step s. Say it started at time step $s-S' < s-S$ with $f_{min}(s-S') > f_{min}(s-S)$, and has covered a larger spatial region $R' \sim S'^{1/D}$. Such an avalanche will contain the avalanche that started at time step $s-S$ as one of its subavalanches. Active sites at time steps s and $s-1$ will obviously belong to the bigger spatial region of size R' as well. The importance of the backward avalanche is that it automatically selects the *smallest* forward avalanche containing both sites $\vec{r}_{min}(s-1)$ and $\vec{r}_{min}(s)$ and, therefore, imposes the most restrictive constraint on their relative positions.

For the evolution model, we proceed by showing that (1) the position of activity $\vec{r}_{min}(s)$ at time step s is equally likely to be at one of the n_{cov} sites with new random numbers; (2) it is uncorrelated with the previous position of the active site $\vec{r}_{min}(s-1)$, within the set of n_{cov} sites. To do this we will again use the powerful observation that any f_0 avalanche of size S leaves in its wake a set of uncorrelated random numbers. For our avalanche in question we can set f_0 equal to $f_{min}(s)$. Then n_{cov} new numbers are uniformly distributed between f_0 and 1 and are equally likely to host the current global minimum. Looking at the n_{cov} sites at time step $s-1$, just before the update was performed, one observes that almost all of these sites have already acquired their final uncorrelated number between f_0 and 1. The only sites which can potentially be active and, therefore, correlated are $\vec{r}_{min}(s-1)$ itself and its nearest neighbors. Because at the next time step the f_0 avalanche dies out, all $2d+1$ new random numbers created at this last time step must be larger than f_0. They simply join the rest of the n_{cov} sites, which already have their random numbers between f_0 and 1, and become indistinguishable from them. Therefore the position of the active site at time step s is uncorrelated from the particular position, within the set of n_{cov} sites, of the active site at time step $s-1$. This finishes the proof that the current jump of activity $r = |\vec{r}_{min}(s) - \vec{r}_{min}(s-1)|$ for the evolution model is bounded only by the linear size R of the backward avalanche that starts at time step s. We propose that this bound also holds for the other extremal models considered here.

Given this bound, the probability $P_{jump}(r > R_0)$ to have a jump distance r larger than R_0 for large R_0 scales in the same way as the probability to have a backward avalanche of linear size R larger than R_0, or, alternatively, volume S larger than R_0^D. Therefore, $P_{jump}(r > R_0) \sim P_b^{all}(S > R_0^D) = R_0^{-D(\tau_b^{all}-1)}$. Substituting the expression for τ_b^{all} from Eq. (41) into this relation and differentiating with respect to R_0, we get the final expression for the exponent π,

$$\pi = 1 + D(2-\tau) . \tag{45}$$

This expression is in agreement with the result $\pi = 1 + \gamma/\nu = 1 + \nu D(2-\tau)/\nu = 1 + D(2-\tau)$ which was derived for the Sneppen model using different methods in [55]. For invasion percolation, the relation between π and τ_b^{all} was first derived by Roux and Guyon [35]. Unfortunately they had an erroneous expression for τ_b^{all}.

Based on Eq. (45) and our numerical values for D and τ, we predict $\pi = 3.26$ ($\pi = 3.20$) in the one- (two-) dimensional evolution model. We have measured the exponent $\pi = 3.23 \pm 0.02$ (Fig. 25), and Jovanovic *et al.* [42] also measured $\pi = 3.1 \pm 0.2$ in the one-dimensional evolution model. In the one- (two-) dimensional LIM, $\pi = 2.93 \pm 0.01$ (Fig. 26) [$\pi = 2.89 \pm 0.03$ (Fig. 27)]. These results also agree with Eq. (45) and the numerical values we obtained for the exponents D and τ. For

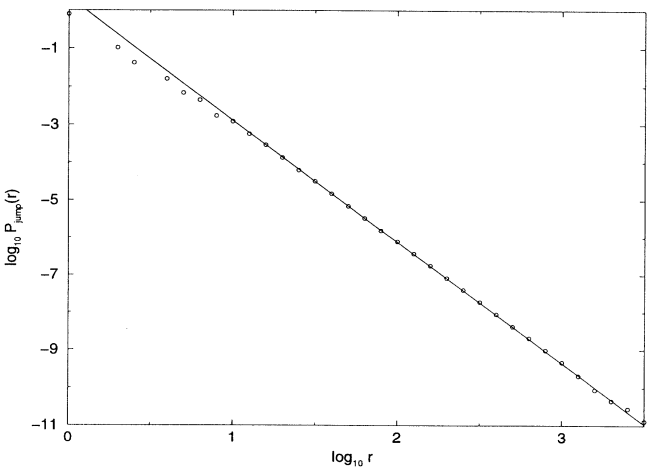

FIG. 25. The distribution of jumps between subsequent minimal sites in the 1D evolution model. The slope of the straight line corresponds to $\pi = 3.23$. We simulated 5×10^7 time steps in the system of size $L = 3000$.

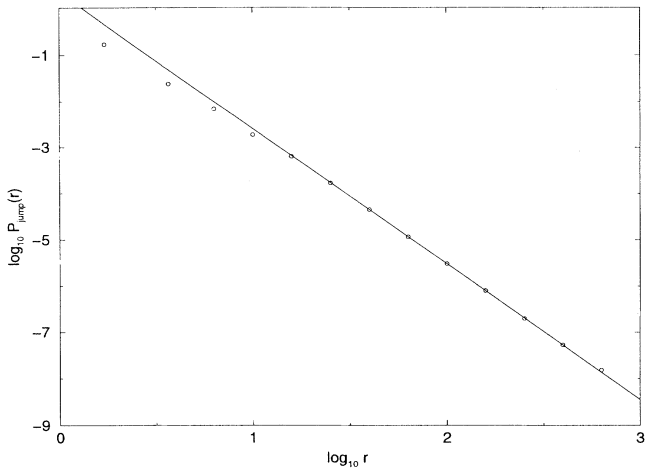

FIG. 26. The distribution of jumps between subsequent minimal sites in the 1D LIM. The slope of the straight line is $\pi = 2.93$. We simulated 5×10^7 time steps in the system of size $L = 3000$.

the one-dimensional Sneppen model, we predict $\pi = 2.21$; Sneppen and Jensen measured $\pi = 2.25 \pm 0.05$ [72], while Tang and Leschhorn measured $\pi = 2.20 \pm 0.05$. In two dimensions, Falk *et al.* [73] measured $\pi = 2.2 \pm 0.2$ consistent with our prediction based on their measured values $\chi = 0.50 \pm 0.03$ and $\tau = 1.45 \pm 0.03$. For IP-3 Furuberg *et al.* measured $\pi = 2.1 \pm 0.1$ [74], which is consistent with their measured value $d_B = 1.37$ and $D = 1.82$ and Eqs. (43) and (45).

V. THE FRACTAL PATTERN OF ACTIVITY

For the SOC extremal models discussed in this article, the dynamics consists of a series of extremal events following one after another. At any given time step s, there is one and only one lattice site where activity occurs. The extremal character of this dynamics lies in the fact that this site is always selected by the *global* minimum (or maximum) of some local driving force. The activity of the model in the critical steady state is highly correlated. It forms an anisotropic fractal in $(d+1)$- (d spatial and one temporal) dimensional space [40]. An example of this fractal activity pattern for the one-dimensional evolution model was shown in Fig. 1. We recall that one characteristic exponent of this fractal is its mass dimension D. This dimension relates S, the total amount of activity within a certain time interval, to the spatial extent, or range of activity, R, through

$$S \sim R^D \ . \tag{46}$$

Due to the sequential character of activity, S is trivially equal to the number of time steps within a selected time interval.

We have already mentioned that in extremal models there exists a purely geometrical fractal property of the pattern of activity. The distribution of distances (Lévy jumps) between subsequent minimal sites, $\vec{r}_{min}(s)$, obeys a power law $P_{jump}(r) \sim r^{-\pi}$. This fractal property was described using backward avalanches in Sec. IV E.

The pattern of activity has another feature where cuts in different directions are fractals themselves. Since the pattern is anisotropic, cuts in different directions have different mass dimensions. The cuts in the spatial direction, at an arbitrary point in time s, are in fact trivial: there is only one active site at any given time. Each cut has exactly one point of activity. The fractal properties of cuts in the time direction s at a given point in space are more interesting. Looking at Fig. 1, one can see that the activity has a tendency to revisit sites. At any given site, the activity is recurrent in time, and can be considered to be a "fractal renewal process" [75]. The collection of return points on the one-dimensional time axis forms a fractal with dimension $0 \leq \tilde{d} \leq 1$. As in earlier sections, we assume that the projection of the activity pattern onto the original d-dimensional lattice forms a dense, compact region of dimension d. Thus we can consider the activity pattern within a spatial region R^d to be composed of R^d one-dimensional fractal time lines. In order to encompass all of the activity, each time line has a length $\sim R^D$. The number of points of the activity cluster which fall on any given time line scales as $\tilde{d}$. Here, we assume also that there is only one dimension $\tilde{d}$ and no multifractal properties of these points on each time line. Thus the quantity $R^d R^{D\tilde{d}}$, the total number of active sites in all time lines, must scale in the same way as the mass of the entire cluster, $S \sim R^D$. This gives an exponent relation:

$$\tilde{d} = 1 - d/D \ . \tag{47}$$

Note that the exponent $\tilde{d}$ is not defined for IP.

Complex spatiotemporal fractal patterns also can be observed in non-SOC systems when their parameters are fine tuned so that they become critical. These avalanche patterns again are characterized by the fractal dimen-

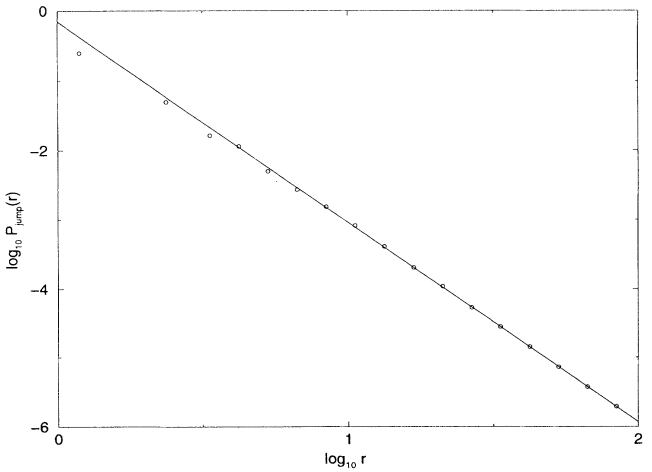

FIG. 27. The distribution of jumps between subsequent minimal sites in the 2D LIM. The slope of the straight line corresponds to $\pi = 2.89$. We simulated 10^9 time steps in a system of size 300×300.

sions of different cuts. Exponent relations analogous to Eq. (47) are obtained below.

For example, let us consider a large, finite directed percolation cluster on a $(d+1)$-dimensional lattice. A part of such a cluster is shown in Fig. 28 for $d = 1$. This cluster is asymmetric with respect to the t direction. Recall that in DP all sites are updated in parallel, so that $t \to t+1$ when all $n(t)$ sites have been advanced. Self-similarity requires that the duration T scales with the spatial extent in any one of the d directions perpendicular to time, R, as $T \sim R^z$ where z is the usual dynamical exponent relating space and time. The total size of the cluster, S, scales with the spatial extent as $S \sim R^D$, where D is the avalanche dimension. Unlike the previous sequential example, we now have more than one active site at a given time step. Thus T and S represent different quantities and the corresponding exponents z and D relating them to spatial size R are not equal to each other. In order to compute D, usually the cluster is partitioned into R^z equal time slices. Each such slice contains $n_{act} \sim R^{d_{act}}$ points of the cluster. This method of partitioning the cluster gives $R^D \sim R^z R^{d_{act}}$, so the avalanche dimension is given by $D = z + d_{act}$. As in the previous example, the avalanche cluster can be composed as R^d one-dimensional fractals, parallel to the time axis, which each contain $T^{\tilde{d}}$ parts of the cluster. Consequently,

$$R^D \sim R^d R^{z\tilde{d}}, \quad \tilde{d} = \frac{D-d}{z} . \tag{48}$$

Note that this relation contains Eq. (47) as a limiting case when $z = D$ and $d_{act} = 0$ (one active site at any given time step).

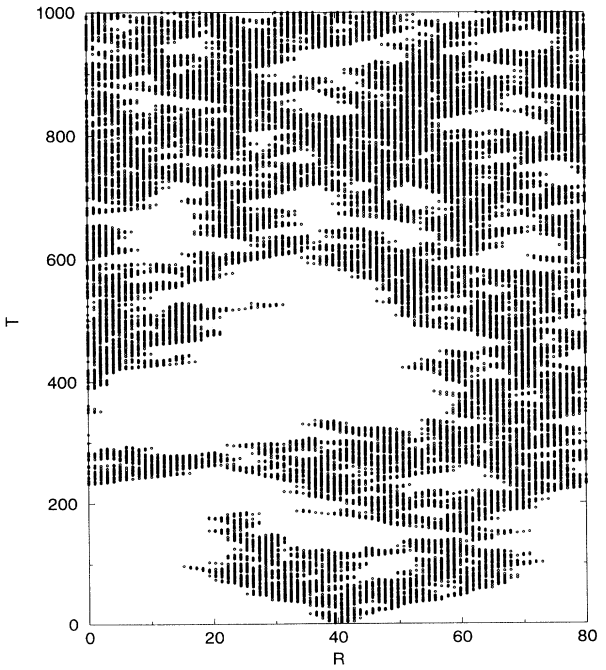

FIG. 28. The pattern of active sites in (1+1)-dimensional bond directed percolation.

Knowledge of the exponent $\tilde{d}$ enables us to calculate two important distributions characterizing return times of activity to a given point in space. As a result, it also characterizes the power spectrum of local activity. The first return probability distribution $P_{FIRST}(\tilde{t})$ is the distribution of "hole" sizes, or intervals, separating subsequent return points of activity. Here $\tilde{t}$ is the size of the hole (either in parallel time t or sequential time s). This distribution is normalizable; $\int_0^\infty P_{FIRST}(\tilde{t})d\tilde{t} = 1$. The average total number of return points, $n(T)$, in an interval of length T is given by the fractal dimension of return points as $n(T) \sim T^{\tilde{d}}$. It can be related to the first return probability

$$n(T) = T - n(T)\int_1^T P_{FIRST}(\tilde{t})\tilde{t}d\tilde{t} ,$$

where

$$P_{FIRST}(\tilde{t}) \sim \tilde{t}^{-\tau_{FIRST}} \text{ for } \tilde{t} \gg 1 . \tag{49}$$

If $\tau_{FIRST} \leq 2$ then the divergence at the upper limit must cancel the T term, so that $T \sim n(T)T^{2-\tau_{FIRST}}$. This leads to the scaling relation

$$\tilde{d} = \tau_{FIRST} - 1 , \tag{50}$$

connecting the fractal dimension of return points to the distribution of hole sizes.

The second distribution $P_{ALL}(\vec{r},\tilde{t})$ is the probability that activity at position 0 at time 0 will be at $\vec{r}$ at time $\tilde{t}$. This quantity does not obey the same normalization condition as P_{FIRST}. Instead $\int P_{ALL}(\vec{r},\tilde{t})d\vec{r} = N$, where N is the average number of active sites. $P_{ALL}(0,\tilde{t})$ is the probability for the activity at time $\tilde{t}$ to revisit a site that was visited at time 0. Unlike $P_{FIRST}(\tilde{t})$ it does not require that the return is the first return of activity, so it is often referred to as the distribution of *all return* times. Since $n(T)$ is simply the sum of all returns of activity to a particular site up to time T, we have

$$n(\tilde{t}+1) - n(\tilde{t}) = P_{ALL}(0,\tilde{t}) . \tag{51}$$

Assuming a power-law form $P_{ALL}(0,\tilde{t}) \sim \tilde{t}^{-\tau_{ALL}}$ for $\tilde{t} \gg 1$, one gets for τ_{ALL}

$$\tilde{d} = 1 - \tau_{ALL} . \tag{52}$$

Comparing Eqs. (50) and (52) gives the general relation

$$\tau_{FIRST} + \tau_{ALL} = 2 \text{ for } \tau_{FIRST} \leq 2 \tag{53}$$

connecting the "lifetime" exponents for the first and all returns of activity.

Recently, Ito [76] has examined the International Seismological Center data of California earthquakes and has found that the "all" and "first" return time distributions for earthquakes to return to a given location are power laws over approximately two decades with characteristic exponents that obey Eq. (53), i.e., $\tau_{FIRST} \approx 1.4$ and $\tau_{ALL} \approx 0.5$. In addition, he found that the distribution of jumps between subsequent hypocenters of earthquakes

may also be a power law with an exponent $\pi \approx 1.7$. This is a remarkable demonstration of the generality of our results.

A. $1/f$ noise and punctuated equilibria

Since $P_{ALL}(0,\tilde{t})$ is the autocorrelation function of the activity, the power spectrum is simply

$$S(f) = \int_{-\infty}^{+\infty} P_{ALL}(0,\tilde{t}) e^{2\pi i f \tilde{t}} d\tilde{t} \sim \frac{1}{f^{\tilde{d}}} . \qquad (54)$$

The mathematical relationship between return times and the power spectrum was derived previously using different methods by Lowen and Teich [75]. Here we have shown that $1/f$ type noise emerges naturally in both self-organized and non-self-organized critical systems as a consequence of avalanche dynamics. As a result, the actual exponent $\tilde{d}$ that characterizes the noise is determined by the dimension D of the avalanches. Equations (47), (48), and (54) establish a formal connection between $1/f$ noise and fractal scaling behavior, i.e., spatiotemporal complexity, in both tuned and self-organized critical models.

Model dependent behavior occurs between the upper critical and lower critical dimension. In the mean field limit, or above the upper critical dimension, the activity is barely able to return and $\tau_{FIRST} = \tau_{ALL} = 1$. As a result, the power spectrum $S(f) \sim 1/f^0$ corresponds to white noise. On the other hand, at the lower critical dimension, the activity becomes dense in time and $\tilde{d} \to 1$. In this case, the power spectrum $S(f) \sim 1/f$, with logarithmic corrections.

Equations (47)–(54) were checked by numerical simulations. We simulated bond DP on a square lattice in 1+1 dimensions at $f = 0.6445$ for $L = 3000$. The data shown in Fig. 29, $\tau_{FIRST} \simeq 1.86$ and $\tau_{ALL} \simeq 0.14$, are in agreement with the theoretical prediction $\tau_{FIRST} = 1.84 \pm 0.02$ and $\tau_{ALL} = 0.16 \pm 0.02$ based on the exponents D and z in Ref. [77]. Also $S(f) \sim 1/f^{0.84}$ in 1+1 dimensions. In $d = 1$ we simulated the BS branching process at branching probability $f = 0.667$ and averaged over $\approx 10^9$ mutations to obtain Fig. 30. Our measured values are $\tau_{FIRST} = 1.58 \pm 0.02$ and $\tau_{ALL} = 0.42 \pm 0.02$, quite close to the predicted values 1.59 and 0.41, respectively. Similar results were found for $d = 2$, at branching probability $f = 0.390$, $\tau_{FIRST} \simeq 1.28$ and $\tau_{ALL} \simeq 0.70$, to be compared with 1.31 and 0.69 from the formulas above. The predicted power spectrum is $S(f) \sim 1/f^{0.59}$ in $d = 1$ and $S(f) \sim 1/f^{0.31}$ in $d = 2$. We measured the power spectrum $S(f) \sim 1/f^{0.58}$ for the one-dimensional evolution model as shown in Fig. 31(a), and $S(f) \sim 1/f^{0.31}$ for the two-dimensional evolution model, as shown in Fig. 31(b).

The evolution model was introduced in an attempt to model punctuated equilibria in biological evolution. Figure 32 shows the accumulated number of activations, or

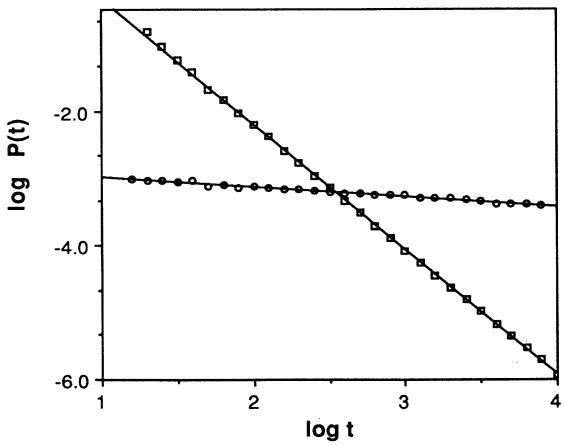

FIG. 29. Distribution of return times for bond DP on a square lattice for $f = 0.6445$ and $L = 3000$. The asymptotic slopes give $\tau_{FIRST} \simeq 1.86$ and $\tau_{ALL} \simeq 0.14$.

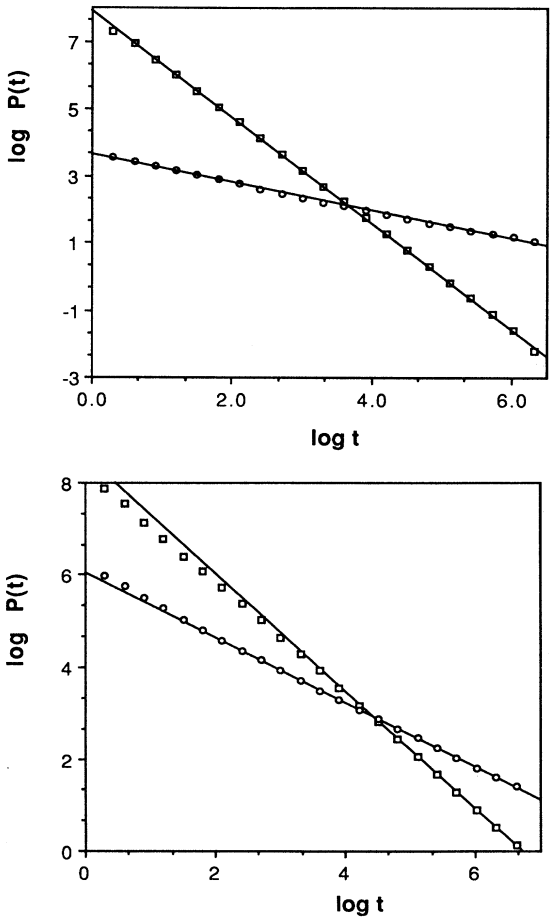

FIG. 30. Return times for the BS branching process. (a) 1D process at branching probability $f = 0.667$ averaged over $\approx 10^9$ mutations. The corresponding exponents are $\tau_{FIRST} \simeq 1.58$ and $\tau_{ALL} \simeq 0.42$. (b) 2D process at $f = 0.3289$ averaged over $\approx 10^9$ mutations. $\tau_{FIRST} \simeq 1.28$ and $\tau_{ALL} \simeq 0.70$.

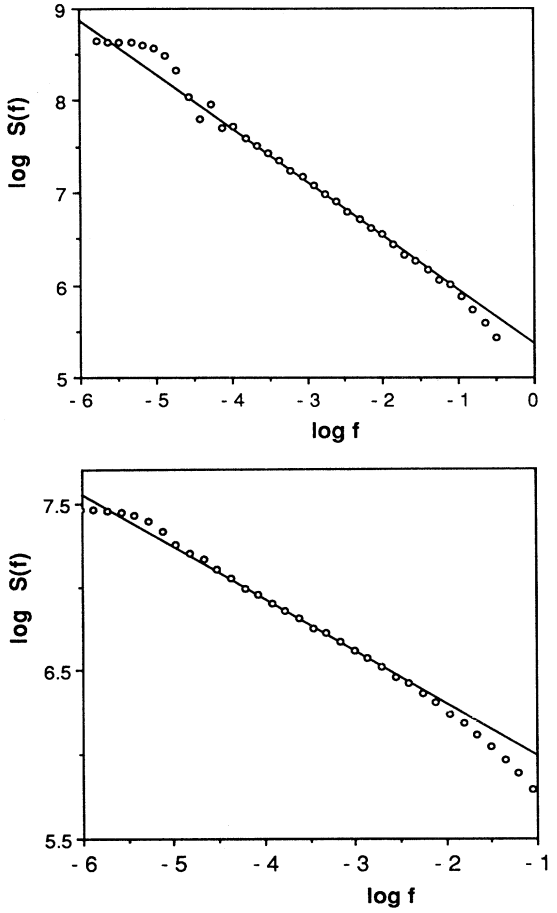

FIG. 31. Power spectrum for (a) the one- and (b) the two-dimensional evolution model.

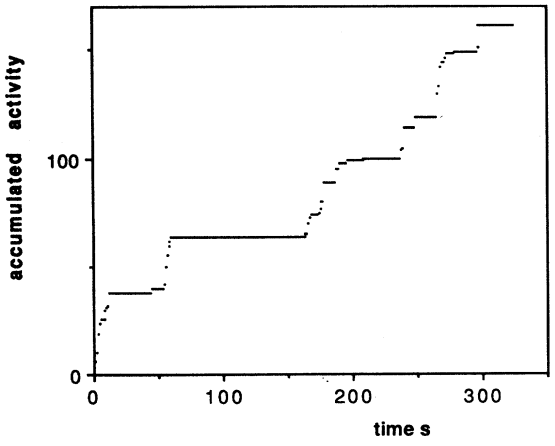

FIG. 32. Punctuated equilibria. The curve shows the accumulated number of times a specific site is visited, or is the minimal site, in the one-dimensional evolution model. This would roughly correspond to the accumulated number of mutations in a particular species. The pattern of change is stepwise rather than being smooth.

returns to a given site, for the one-dimensional evolution model. In terms of the model, these accumulated returns would roughly correspond to accumulated mutations in a given species. The resulting devil's staircase shows plateaus of stasis interrupted by bursts of activity. The plateaus have a power-law distribution in sizes decaying as $S^{-\tau_{FIRST}}$. This staircase behavior is qualitatively similar to the punctuated equilibrium behavior observed for the evolution of real species [13]. This suggests that the punctuations for a single species are correlated to the avalanches in the global ecology.

VI. INTERFACE DEPINNING

So far, the main emphasis in this article has been on a class of extremal SOC models. In Sec. IV, we started comparing these extremal models with their constant force parallel counterparts, where all currently active sites are updated in parallel at each time step. Here we discuss the relationship between tuned and SOC models of interface depinning in more detail.

The behavior of an interface driven in the presence of quenched random pinning forces appears in a wide variety of contexts. These include, among others, fluid invasion in a porous medium [59], the motion of magnetic domain walls [61], flux lines, or charge density waves [17,78,79] in the presence of quenched disorder. The depinning transition in the charge density wave system has previously been described in terms of avalanche dynamics in sandpile models [17,79]. The notion of an external force can be easily incorporated into the rules of the models we have discussed. Applying an external force f_0 means moving in parallel all sites having their local "depinning" force $f_i < f_0$. Below the threshold force f_c, the interface is pinned in one of many possible metastable states. An external force greater than the threshold causes the interface to move with a finite average velocity which vanishes continuously at a depinning transition. The instantaneous velocity, proportional to the density of active sites, fluctuates in time around its average value.

Instead of tuning the force to the depinning threshold, the velocity may be tuned. In this case, the force fluctuates in time, in such a way that the instantaneous velocity is constant. The depinning transition at constant velocity is reached as the limit when the imposed velocity vanishes. The instantaneous interface velocity in discrete lattice models is simply proportional to the current density of active sites: $v = cn_{act}/L^d$, where c is a constant of $O(1)$. We restore the rules of SOC extremal interface models if we require that strictly one site is moving at any given time step and this site is selected as the most unstable in the whole system, i.e., the global minimum of f_i. This corresponds to the interface velocity $v_{ext} = cL^{-d}$. Some of the critical properties of the model driven at constant velocity are the same as at constant force but others are different. It is interesting to note that Wilkinson and Willemsen [33] introduced invasion percolation as a modification of earlier models

[34] that were driven at constant force. As they noted, the introduction of extremal dynamics corresponds to the constant *velocity* invasion process in the limit of vanishing velocity.

Theoretical studies of interface depinning have concentrated along two main directions. One theoretical approach has been to apply a functional renormalization group procedure to a variety of different depinning phenomena [79,80]. This has yielded both perturbative results and results that have been claimed to be exact. For example, for the LIM defined by Eq. (1), it has been claimed [65] that the roughness exponent $\chi = (4-d)/3$ exactly. Another theoretical approach has been to consider simple lattice models for these phenomena, which may, due to their simplicity, be analytically tractable.

Several of the parallel lattice models defined in Sec. II describe interface depinning at constant force. The LIM and TLB model presumably describe the depinning of magnetic domain walls having purely linear force terms, and other elastic interfaces having nonlinear force terms, respectively [81]. Sneppen was the first to introduce a self-organized critical extremal model dedicated to interface depinning; similarly a SOC, or constant velocity, variant of the LIM model can be constructed [40]. The general properties of these SOC models have been analyzed in the preceding sections. Our main results were the derivation of two exact equations, a stationarity condition, and numerous exponent relations. These scaling relations are summarized in Table I.

We now discuss how our results may be generalized to the tuned depinning models driven by constant external force. Here, we only analyze the behavior as the depinning transition is approached from below. In this limit, we will show that the tuned and SOC variants have the same avalanche dimension D, the same avalanche distribution exponent τ, and the same roughness exponent χ. However, the exponents that describe propagating activity within avalanches are different. In particular, the stationarity law $\eta = 0$ does not necessarily hold for the tuned models at constant force, although it does hold for the extremal SOC models. This implies that the fractal dimension of activity d_f and the dynamical exponent z can also be different in these two cases. These results are verified numerically.

We first concentrate on the case of the Sneppen and TLB models which are constant velocity and constant force versions of the same depinning phenomenon. Let us recall the definition of the f_0 avalanche in the Sneppen model. This avalanche intervenes between subsequent punctuations of the barrier f_0 by the signal $f_{min}(s)$, which is the extremal value of the pinning force. Geometrically, an f_0 avalanche takes the interface from one critical "blocking surface" where all the random numbers are greater than or equal to f_0 to another f_0 blocking surface, as shown in Fig. 3. Tang and Leschhorn [54] showed that in one dimension these blocking surfaces correspond to percolating paths on a directed percolation cluster, formed by all sites with $f_i < f_0$. Given a collection of random pinning forces $f(\vec{x}, h)$, and an initial interface configuration identifying with a critical blocking surface, the next blocking surface that is encountered under Sneppen dynamics is the same blocking surface that would be encountered in an equivalent parallel model, i.e., the TLB model, driven with an applied force f_0. The order in which the sites between these two blocking surfaces are invaded is completely different, though. In the Sneppen model, one always chooses the smallest random pinning force, f_{min}. In the TLB model, one advances all sites where $f_i \leq f_0$ in parallel. Nevertheless, the difference between the initial interface configuration and the final configuration, given by the two blocking surfaces, is the same for the two models. Thus the TLB model has the same threshold f_c, roughness exponent χ of blocking surfaces, and avalanche distribution $P(S, f_0)$. This has been confirmed numerically in Refs. [32,54,62,45,73].

The roughness exponent χ characterizes the saturation width w of the height fluctuations in a system of size L, so that $w^2 = \langle (h - \langle h \rangle)^2 \rangle \sim L^{2\chi}$ [82,83]. The roughness exponent χ and the avalanche dimension D are related via

$$D = d + \chi \,. \tag{55}$$

The logic behind this relation is as follows. (1) The set of sites advanced at least once during the course of an avalanche is assumed to form a compact object having the same dimension d as the interface substrate. In $d = 1$ any connected set is also compact so this assumption is obviously valid. In higher dimensions, we are not aware of any proof that the avalanches are compact. (2) It is assumed that there are no multifractal features of the measure, defined as a total number of updates during an avalanche, on the set of n_{cov} sites. Namely, there is only one scale characterizing the number of times each site covered by the avalanche is updated. If both conditions (1) and (2) are satisfied, the avalanche volume, which in extremal models is simply proportional to its temporal duration S, can be written as $R^d R^\chi$, and the relation (55) is satisfied. On the other hand, it is not completely inconceivable that in high enough dimensions one of the assumptions can be wrong for the interface models. In particular, this would occur in dimensions above the upper critical dimension of the model, if an upper critical dimension exists. Then Eq. (55) no longer holds, and D, the avalanche dimension, can be smaller than d, the dimension of the substrate. The results of the numerical simulations of the TLB model reported in [44,45] suggest that the relation (55) may be valid in dimensions as high as $d = 4$.

Taking into account these assumptions, our results contained in Sec. IV B, which were derived for the Sneppen model, directly apply to its parallel counterpart—the TLB model.

The critical dynamics of the interface as it propagates from one blocking surface to another may be different in the constant velocity (SOC) and constant force interface models. This difference is not restricted to a trivial time redefinition, where in extremal versions the temporal duration of an avalanche is simply proportional to its volume, while in parallel versions these quantities differ because all active sites are advanced in parallel. What is more interesting is that even the fractal dimension d_f

of active sites (sites with $f_i < f_0$) is different in these two cases. Since the dynamics of the Sneppen model is stationary, the dynamical exponent $\eta = 0$. There is no such stationarity condition in the TLB model at constant force; thus η is not necessarily zero in that model. In fact, in one dimension Tang and Leschhorn [62] have argued that $z = 1$ exactly for the TLB model at constant force, in contrast to $z \equiv D - d_f \simeq 1.21$ which is predicted as a corollary of the $\eta = 0$ law for the Sneppen model and which was measured in Fig. 18. In fact, we measured z for the TLB model, as also shown in Fig. 18, and confirmed the $z = 1$ prediction and previous numerical results [62,45]. This demonstrates that the dynamical critical exponents in SOC and tuned critical phenomena can be different.

It is possible, though, that these differences may become smaller or disappear entirely for tuned and SOC versions as the substrate dimension increases. The numerical simulations of the TLB model in dimensions up to $d = 4$ [44,45] may possibly support this point of view. One of the consequences of the $\eta = 0$ law is that the exponents they defined as τ_{surv} and δ would satisfy the relation $\delta = d_f/z = \tau_{surv} - 1$. This relation is obviously violated in the one-dimensional model where they [44] report $\tau_{surv}^{(1+1)} = 1.46(2)$ and $\delta^{(1+1)} = 0.60(3)$, which once again rules out $\eta = 0$ for the one-dimensional TLB model. Their results for higher dimensions $\delta^{(2+1)} = 1.14(6)$, $\tau_{surv}^{(2+1)} = 2.18(3)$, $\delta^{(3+1)} = 1.6(1)$, $\tau_{surv}^{(3+1)} = 2.54(5)$, $\delta^{(4+1)} = 1.9(2)$, and $\tau_{surv}^{(4+1)} = 3.0(2)$, however, seem to obey the $\eta = 0$ relations within their numerical uncertainties. We do not know whether this apparent agreement in dimension $d > 1$ is simply a numerical coincidence.

A similar argument that in tuned and self-organized versions of the model the exponents τ and D are the same, while η in general is different, can be applied to the LIM. In this model, the advancement at any given site can never cause a neighboring unstable site to become stable; the motion at an active site can never destroy another active site. This means that one can interchange, arbitrarily, the order in which the unstable sites move without changing the final metastable configuration that is reached. This property is reminiscent of the Abelian properties of the sandpile model exploited by Dhar [23]. This interchangeability means that the critical force f_c, as well as the exponents D and τ describing the avalanche statistics, are the same for the two versions. Obviously, though, η can be different because the dynamics during an avalanche depends on the way unstable sites move. In fact, Leschhorn measured $z = 1.42 \pm 0.03$ in one dimension and $z = 1.58 \pm 0.04$ in two dimensions for the tuned LIM at constant force; whereas, based on our measured values of D and τ, we predict the quite different values $z \simeq 1.94$ (one dimension) and $z \simeq 2.04$ (two dimensions) for the SOC or constant velocity variant.

For the interface models, it is conventional to assume the validity of the relation (55) and to express the critical exponents in terms of $\chi = D - d$ and ν, the spatial correlation length exponent along the substrate. In this case, Eqs. (31) and (32) can be rewritten in terms of ν and χ as

$$\tau = 1 + \frac{d - 1/\nu}{d + \chi} , \tag{56}$$

$$\gamma = 1 + \chi\nu . \tag{57}$$

In the one-dimensional Sneppen model, ν and χ have been derived from the fractal properties of the (1+1)-dimensional directed percolation cluster [54,55]; namely, $\chi = \nu_\perp^{DP}/\nu_\parallel^{DP}$, and $\nu = \nu_\parallel^{DP}$, where $\nu_\perp^{DP}$ and $\nu_\parallel^{DP}$ are parallel and perpendicular correlation length exponents in (1+1)-dimensional directed percolation. For the one-dimensional Sneppen model, these expressions differ from the predictions of Olami, Procaccia, and Zeitak that $\tau = 2/(2 + \chi)$ and $\gamma = 2$ [66]. The avalanche dimension D was measured for the self-organized LIM as shown in Fig. 33. In $d = 1$, $D = 2.23 \pm 0.03$, and in $d = 2$, $D = 2.725 \pm 0.02$. For the LIM in both one and two dimensions, D was measured by computing, for each backward avalanche, the duration S of the backward avalanche, and the squared distance R^2 from the site starting the backward avalanche to the site ending it. Substituting these measured values into the relation $\chi = D - d$, gives $\chi \simeq 1.23$ in $d = 1$ and $\chi \simeq 0.72$ in $d = 2$. These values for χ are in agreement with numerical simulations by Leschhorn [58], but higher than the prediction $\chi = (4 - d)/3$ from functional renormalization group (RG) calculations [65] in both one and two dimensions.

One might wonder if the one-dimensional LIM describes the behavior of any real physical system. Our measured value of the interface roughness $\chi = 1.23 \pm 0.02$ [40] derived from the avalanche fractal dimension $D = 1 + \chi$, as well as the reported values $\chi = 1.25 \pm 0.01$ [58]

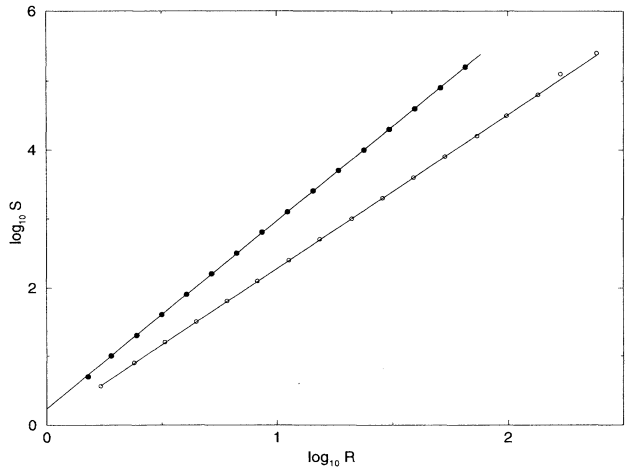

FIG. 33. S vs R from backward avalanches in 1D (open circles) and 2D (filled circles) LIM. In 1D, the slope is $D = 2.23 \pm 0.03$ from simulations of 5×10^7 time steps in the stationary state of a system of size $L = 3000$. In 2D, the slope is $D = 2.725 \pm 0.02$ from simulations of 10^9 time steps in the stationary state of a system of size 300×300.

and $\chi = 1.2 \pm 0.1$ [56], contradict the usual condition that the "self-affine" interface looks flat when viewed at a sufficiently large length scale. It may be more appropriate to call the interfaces with $\chi > 1$ "super-rough" [83,84]. As was suggested in [56], one possible physical realization of the super-rough interface is fluid invasion in a porous medium. Martys, Robbins, and Cieplak [60] introduced an explicit model for this process. They have shown that depending on the wetting properties of the invading fluid in 1+1 dimensions one observes two distinct universality classes of the constant pressure, i.e., force, interface depinning transition. One was identified with the constant pressure version of invasion percolation [34], having an extremely curved interface with overhangs at all length scales. The interface from the other universality class has overhangs only at small length scales, and Roux and Hansen have argued that the 1+1 LIM shares the same universality class [56]. Our numerical results support this conjecture. We have measured $\tau = 1.13 \pm 0.03$ in very good agreement with the measured value $\tau = 1.125 \pm 0.025$ of [60]. Scaling relations analogous to Eqs. (7), (31), and (32) for the non-SOC model were derived in [60] based on the assumption that the avalanches in the model are isotropic; specifically they assumed $D = d + 1$, which is different from our result $D = d + \chi$. Nevertheless, these authors considered the interface itself to be self-affine ($\chi \neq 1$), and not isotropic. Within numerical uncertainty, it appears to us that their results are also consistent with anisotropic super-rough avalanches having the same fractal properties as the interface itself ($\chi = D - d$). For example, inserting their numerical value $\nu = 1.30 \pm 0.05$ and our numerical value $D = 2.23$ into Eq. (56) one gets $\tau = 1.105$, which is also consistent with the measured values cited above. The question of the shape of the avalanches in their model could probably be resolved by direct measurements of the avalanche volume S vs its spatial extent R.

Similar considerations may apply to self-affine interfaces in the (2+1)-dimensional random field Ising model studied by Ji and Robbins [61]. They measured $\tau = 1.28 \pm 0.05$ and $\nu = 0.75 \pm 0.05$ in agreement with our numerical result $\tau = 1.29 \pm 0.02$ for the (2+1)-dimensional LIM and Eq. (56) using $D = 2 + \chi = 2.72 \pm 0.02$. Again, they assumed the avalanches to be isotropic in the random field Ising model, while the avalanches in the LIM are anisotropic and self-affine.

VII. CONCLUSIONS

We have presented a comprehensive theory for avalanche dynamics in evolution, growth, and depinning models. These models are defined in Sec. II and represent different universality classes. We have shown that avalanche dynamics leads to spatiotemporal complexity, and emerges as a result of extremal dynamics in driven systems. Spatiotemporal complexity is manifested in the formation of fractal structures, the appearance of $1/f$ type noise, diffusion with anomalous Hurst exponents, Lévy flights, and punctuated equilibrium behavior. These phenomena can all be related to the same underlying avalanche dynamics.

We present two exact equations for these phenomena. (1) The approach to the critical attractor is governed by a "gap" equation for the divergence of avalanche sizes. (2) The average number of sites covered by the avalanche can be related to the average size of avalanches. If there is a power-law divergence for the average avalanche size, then the number of sites covered by an avalanche diverges with exponent -1. In addition, the conservation of activity in the stationary state manifests itself through the fundamental relation $\eta = 0$. It follows that many of the critical exponents in a class of SOC extremal models can be derived from two basic exponents.

These exponent relations are summarized in Table I. Depending on the model it may be more convenient to use one or another basic set of two exponents. In Table I we write our exponent relations in terms of two such basic sets: (D, ν) or (D, τ). The scaling relations are defined for the Bak-Sneppen evolution model, the Sneppen model for SOC interface depinning, the Zaitsev flux creep model, a SOC "linear" interface model, and invasion percolation. The horizontal lines separate results from different sections of this article.

Our results from numerical simulations are summarized in Table II. This table contains the expressions for the exponents of the one- and two-dimensional Bak-Sneppen model, one- and two-dimensional LIM, and the one-dimensional Sneppen model based on *direct* numerical simulations. The overall consistency between the exponent relations from Table I and the numerical results in Table II demonstrates the validity of our scaling relations. Most of the numerical results from Table II were illustrated in figures throughout the text.

Some of these scaling relations show that $1/f$ noise and spatial fractal behavior can be unified and have a natural explanation in terms of avalanche dynamics in both SOC and non-SOC systems. The pattern of avalanches in the critical state can be described as a fractal in d spatial plus one temporal dimension, with mass dimension D. Temporal behavior, such as $1/f$ noise in the power spectrum, and spatial long-range correlations can be formally related as different cuts in the same underlying fractal. In the stationary state, time reversal symmetry is broken, so that forward and backward avalanches have different statistics. We derive a scaling relation for the Lévy distribution of jumps in the SOC extremal models. Finally, we point out the similarities and differences between interface depinning at constant velocity (SOC) and constant force.

ACKNOWLEDGMENTS

This work was supported by the U.S. Department of Energy Division of Materials Science, under Contract No. DE-AC02-76CH00016. M.P. thanks the U.S. Department of Energy Distinguished Postdoctoral Research Program for financial support. The authors thank K. Sneppen for useful conversations and B. Drossel for helpful comments on the manuscript.

APPENDIX: INVASION PERCOLATION

Invasion percolation is very sensitive to the definition of the boundary of the invaded cluster. In one version of the model, the boundary consists of any site having at least one nearest neighbor in the invaded cluster. The boundary defined by this rule includes sites on the external perimeter of the invaded cluster as well as sites on the perimeter of numerous "lakes" in the interior of the cluster. The invaded cluster in this model from time to time exactly identifies itself with the infinite cluster of ordinary percolation. At these instances, all of the random numbers on the boundary are uniformly distributed above the "gap" f_c, where f_c is the critical density of ordinary percolation. In two dimensions, the whole boundary of the cluster of ordinary percolation has a fractal dimension d_B equal to the fractal dimension D of the cluster itself, and $D = d_B = 91/48 \simeq 1.89$ [14]. We will refer to the invasion percolation model with the boundary defined in this manner as IP-1.

An important physical realization of invasion percolation is the displacement of one fluid by another in a porous medium. In this case, once a region of noninvaded fluid is completely surrounded by the invading fluid, no further invasion can take place on this part of the boundary due to incompressibility. This event, known as self-trapping, can be taken into account in the invasion percolation model by changing the definition of the active boundary. With self-trapping, only the sites touching the *external perimeter* of the invaded region comprise the active boundary. It is believed that self-trapping does not change the fractal dimension of the invaded cluster in two dimensions [14]. In ordinary two-dimensional percolation, it is known that the external perimeter of the cluster has a smaller fractal dimension than the cluster itself, i.e., $d_B < D$. Depending on the details of the precise definition of the external perimeter, one gets $d_B = 7/4 = 1.75$ [85] or $d_B = 4/3 \simeq 1.33$ [86]. These different definitions thus give different variants of the invasion percolation model, which we will refer to as IP-2 and IP-3, respectively.

In Sec. III we used the result by Roux and Guyon [35] for the scaling of the boundary of the growing IP cluster with its volume. For the sake of completeness, we reproduce their arguments. During the transient, the invaded cluster can be characterized by a growing correlation length ξ. Since the growth starts from a d-dimensional base of the $(d+1)$-dimensional hypercube, the natural scaling form for the invaded volume s is

$$s \sim (L/\xi)^d \xi^D \ , \tag{A1}$$

and for the boundary of invaded cluster $b(s)$,

$$b(s) \sim (L/\xi)^d \xi^{d_B} \ . \tag{A2}$$

Combining these two equations we get

$$b(s)/L^d = (s/L^d)^{\frac{d_B-d}{D-d}} \ , \tag{A3}$$

and therefore $g = \frac{d_B-d}{D-d}$.

It is interesting to note that the simplest assumption that the effective distance from the critical point scales as $f_c - G(s) \sim \xi^{-1/\nu} \sim (s/L^d)^{-1/\nu(D-d)}$ agrees with the gap equation after we substitute into it the expression for g and for γ. This once more confirms the overall consistency of our scaling relations.

[1] Y.-C. Zhang, J. Phys. (France) I **1**, 971 (1991); H.C. Fogedby, J. Stat. Phys. **69**, 411 (1992).
[2] B.B. Mandelbrot, *The Fractal Geometry of Nature* (Freeman, New York, 1983).
[3] P.H. Coleman, L. Pietronero, and R.H. Sanders, Astron. Astrophys. **200**, L32 (1988); L. Pietronero, Physica A **144**, 257 (1987).
[4] A. Rinaldo, I. Rodriguez-Iturbe, R. Rigon, E. Ijjasz-Vasquez, and R.L. Bras, Phys. Rev. Lett. **70**, 822 (1993).
[5] *Fractals in the Earth Sciences,* edited by C.C. Barton and P.R. Lapointe (Plenum, New York, 1994).
[6] W.H. Press, Comments Astrophys. **7**, 103 (1978).
[7] See, for example, the empirical observations of H.E. Hurst described in Refs. [2] and [14].
[8] F. Gruneis, M. Nakao, and M. Yamamoto, Biol. Cybernetics **62**, 407 (1990).
[9] B. Gutenberg and C.F. Richter, Ann. Geofis. **9**, 1 (1956).
[10] E. Somfai, A. Czirok, and T. Vicsek, J. Phys. A **27**, L757 (1994).
[11] V. Frette, K. Christensen, A. Malthe-Sorensen, J. Feder, T. Jossang, and P. Meakin (unpublished).
[12] S. Field, J. Witt, F. Nori, and X. Ling, Phys. Rev. Lett. **74**, 1206 (1995).
[13] S.J. Gould and N. Eldredge, Paleobiology **3**, 114 (1977); Nature **366**, 223 (1993).
[14] J. Feder, *Fractals* (Plenum, New York, 1989).
[15] H. Bai-Lin, *Chaos* (World Scientific, Singapore, 1984).
[16] P. Bak, C. Tang, and K. Wiesenfeld, Phys. Rev. Lett. **59**, 381 (1987); Phys. Rev. A **38**, 364 (1988); P. Bak and M. Creutz, in *Fractals and Disordered Systems,* edited by A. Bunde and S. Havlin (Springer, Berlin, 1994), Vol. II; P. Bak and M. Paczuski, Phys. World **6** (12), 39 (1993).
[17] C. Tang and P. Bak, Phys. Rev. Lett. **60**, 2347 (1988).
[18] P. Bak and C. Tang, J. Geophys. Res. B **94**, 15 635 (1989); Z. Olami, H.J.S. Feder, and K. Christensen, Phys. Rev. Lett. **68**, 1244 (1992); K. Christensen and Z. Olami, Phys. Rev. A **46**, 1829 (1992).
[19] J.M. Carlson, J.T. Chayes, E.R. Grannan, and G.H. Swindle, Phys. Rev. Lett. **65**, 2547 (1990).
[20] P. Bak, K. Chen, and C. Tang, Phys. Lett. A **147**, 297 (1990); B. Drossel and F. Schwabl, Phys. Rev. Lett. **69**, 1629 (1992).
[21] B. Drossel, S. Clar, and F. Schwabl, Phys. Rev. Lett. **71**, 3739 (1993).
[22] M. Paczuski and P. Bak, Phys. Rev. E **48**, R3214 (1993).
[23] D. Dhar, Phys. Rev. Lett. **64**, 1613 (1990); D. Dhar and S.N. Majumdar, J. Phys. A **23**, 4333 (1990); S.N. Majumdar and D. Dhar, Physica A **185**, 129 (1992).

[24] D. Dhar and R. Ramaswamy, Phys. Rev. Lett. **63**, 1659 (1989).
[25] L. Pietronero, A. Erzan, and C. Evertsz, Phys. Rev. Lett. **61**, 861 (1988); Physica A **151**, 207 (1988); R. Cafiero, L. Pietronero, and A. Vespignani, Phys. Rev. Lett. **70**, 3939 (1993).
[26] T.A. Witten and L.M. Sander, Phys. Rev. Lett. **47**, 1400 (1981).
[27] L. Pietronero, A. Vespignani, and S. Zapperi, Phys. Rev. Lett. **72**, 1690 (1994); A. Vespignani, S. Zapperi, and L. Pietronero, Phys. Rev. E **51**, 1711 (1995).
[28] M. Marsili, Europhys. Lett. **28**, 385 (1994).
[29] S.I. Zaitsev, Physica A **189**, 411 (1992).
[30] S.L. Miller, W.M. Miller, and P.J. McWhorter, J. Appl. Phys. **73**, 2617 (1993).
[31] P. Bak and K. Sneppen, Phys. Rev. Lett. **71**, 4083 (1993).
[32] K. Sneppen, Phys. Rev. Lett. **69**, 3539 (1992) .
[33] D. Wilkinson and J.F. Willemsen, J. Phys. A **16**, 3365 (1983).
[34] R. Lenormand, C.R. Acad. Sci. Ser. B **291**, 279 (1980); R. Chandler, J. Koplik, K. Leman, and J. Willemsen, J. Fluid Mech. **119**, 249 (1982).
[35] S. Roux and E. Guyon, J. Phys. A **22**, 3693 (1989).
[36] S. Maslov, Phys. Rev. Lett. **74**, 562 (1995).
[37] M. Paczuski, S. Maslov, and P. Bak, Brookhaven National Laboratory Report No. BNL-49916, 1993 (unpublished); Europhys. Lett. **27**, 97 (1994).
[38] M. Paczuski, S. Maslov, and P. Bak, Europhys. Lett. **28**, 295 (1994).
[39] M. Paczuski, P. Bak, and S. Maslov, Phys. Rev. Lett. **74**, 4253 (1995).
[40] S. Maslov, M. Paczuski, and P. Bak, Phys. Rev. Lett. **73**, 2162 (1994).
[41] P. Grassberger, Phys. Lett. A **200**, 277 (1995), and unpublished.
[42] B. Jovanovic, S.V. Buldyrev, S. Havlin, and H.E. Stanley, Phys. Rev. E **50**, 2403 (1994).
[43] P. Sornette, J. Phys. (France) I **4**, 209 (1994).
[44] L.A.N. Amaral *et al.*, Phys. Rev. E **51**, 4655 (1995).
[45] S.V. Buldyrev *et al.*, Phys. Rev. A **45**, R8313 (1992); Physica A **200**, 200 (1993).
[46] M. Kardar, G. Parisi, and Y.-C. Zhang, Phys. Rev. Lett. **56**, 889 (1986).
[47] T. Hwa and M. Kardar, Phys. Rev. Lett. **62**, 1813 (1989); G. Grinstein, D.-H. Lee, and S. Sachdev, *ibid.* **64**, 1927 (1990).
[48] M. Paczuski, Phys. Rev. E **52**, 2137 (1995).
[49] K. Sneppen, P. Bak, H. Flyvbjerg, and M.H. Jensen, Proc. Natl. Acad. Sci. U.S.A. **92**, 5209 (1995); P. Bak and M. Paczuski, *ibid.* **92**, 6689 (1995).
[50] H. Flyvbjerg, K. Sneppen, and P. Bak, Phys. Rev. Lett. **45**, 4087 (4087).
[51] T.S. Ray and N. Jan, Phys. Rev. Lett. **72**, 4045 (1994).
[52] J. de Boer, B. Derrida, H. Flyvbjerg, A.D. Jackson, and T. Wettig, Phys. Rev. Lett. **73**, 906 (1994); J. de Boer, A.D. Jackson, and T. Wettig, Phys. Rev. E **51**, 1059 (1995).
[53] S. Boettcher and M. Paczuski (unpublished).
[54] L.-H. Tang and H. Leschhorn, Phys. Rev. Lett. **70**, 3832 (1993); H. Leschhorn and L.-H. Tang, Phys. Rev. E **49**, 1238 (1994).
[55] S. Maslov and M. Paczuski, Phys. Rev. E **50**, R643 (1994).
[56] S. Roux and A. Hansen, J. Phys. (France) I **4**, 515 (1994).
[57] S.F. Edwards and D.R. Wilkinson, Proc. R. Soc. London Ser. A **381**, 17 (1982).
[58] H. Leschhorn, Physica A **195**, 324 (1993).
[59] M.A. Rubio, C.A. Edwards, A. Dougherty, and J.P. Gollub, Phys. Rev. Lett. **63**, 1685 (1989).
[60] N. Martys, M.O. Robbins, and M. Cieplak, Phys. Rev. B **44**, 12 294 (1991).
[61] R. Bruinsma and G. Aeppli, Phys. Rev. Lett. **52**, 1547 (1984); H. Ji and M.O. Robbins, Phys. Rev. B **46**, 14 519 (1992).
[62] L.-H. Tang and H. Leschhorn, Phys. Rev. A **45**, R8309 (1992).
[63] D. Stauffer, *Introduction to Percolation Theory* (Taylor, London, 1985); G. Grimmett, *Percolation* (Springer, New York, 1989).
[64] I. Jensen and R. Dickman, Phys. Rev. E **48**, 1710 (1993).
[65] O. Narayan and D.S. Fisher, Phys. Rev. B **48**, 7030 (1993).
[66] Z. Olami, I. Procaccia, and R. Zeitak, Phys. Rev. E **49**, 1232 (1994); Phys. Rev. E **52**, 3402 (1995).
[67] K. Sneppen (private communication).
[68] The exponent relations derived in this section can be generalized to the case where the set of covered sites forms a fractal of dimension $d_{cov} < d$ rather than being compact. This is accomplished by replacing d with d_{cov} in all formulas in this section.
[69] J.F. Gouyet, Physica A **168**, 581 (1990).
[70] P. Grassberger and A. de la Torre, Ann. Phys. (N.Y.) **122**, 373 (1979).
[71] Note that our definition of η differs from the usual definition of η, which is defined with respect to parallel time, as in Ref. [70], and which we refer to as η_t. The quantity which we call η is equal to $z\eta_t/D$.
[72] K. Sneppen and M.H. Jensen, Phys. Rev. Lett. **71**, 101 (1993).
[73] J. Falk, M.H. Jensen, and K. Sneppen, Phys. Rev. E **49**, 2804 (1994).
[74] L. Furuberg, J. Feder, A. Aharony, and T. Jossang, Phys. Rev. Lett. **61**, 2117 (1988).
[75] S.B. Lowen and M.C. Teich, Phys. Rev. E **47**, 992 (1993).
[76] K. Ito, Phys. Rev. E **52**, 3232 (1995).
[77] J.W. Essam, K. De'Bell, J. Adler, and F. Bhatti, Phys. Rev. B **33**, 1982 (1986).
[78] N.P. Ong and P. Monceau, Phys. Rev. B **18**, 5272 (1978); R.M. Fleming and C.C. Grimes, Phys. Rev. Lett. **42**, 1423 (1979); P.A. Lee and T.M. Rice, Phys. Rev. B **19**, 3970 (1979).
[79] O. Narayan and A. Middleton, Phys. Rev. B **49**, 244 (1994).
[80] T. Nattermann, S. Stepanow, L.-H. Tang, and H. Leschhorn, J. Phys. (France) II **2**, 1483 (1992); O. Narayan and D.S. Fisher, Phys. Rev. B **46**, 11 520 (1992); D. Ertas and M. Kardar, Phys. Rev. E **49**, R2532 (1994).
[81] S. Galluccio and Y.-C Zhang, Phys. Rev. E **51**, 1686 (1995).
[82] F. Family and T. Viscek, J. Phys. A **18**, L75 (1985).
[83] T. Halpin-Healy and Y.-C. Zhang, Phys. Rep. **254**, 215 (1995).
[84] S. Das Sarma, S.V. Chaisas, and J.M. Kim, Phys. Rev. E **49**, 122 (1994).
[85] H. Saleur and B. Duplantier, Phys. Rev. Lett. **58**, 2325 (1987).
[86] T. Grossman and A. Aharony, J. Phys. A **19**, L745 (1986).